US Army Corps of Engineers

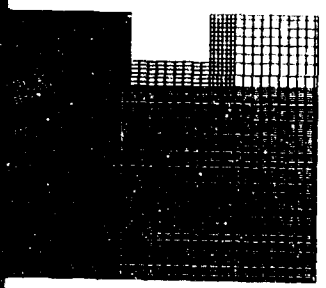

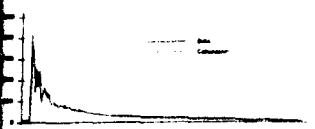

STRUCTURES LABORATORY

TECHNICAL REPORT SL-92-9

PARAMETERS AFFECTING LOADS ON BURIED STRUCTURES SUBJECTED TO LOCALIZED BLAST EFFECTS

by

James T. Baylot

Structures Laboratory

DEPARTMENT OF THE ARMY
Waterways Experiment Station, Corps of Engineers
3909 Halls Ferry Road, Vicksburg, Mississippi 39180-6199

April 1992
Final Report

Approved For Public Release; Distribution Is Unlimited

Prepared for DEPARTMENT OF THE ARMY
Assistant Secretary of the Army (R&D)
Washington, DC 20315

Under In-House Laboratory Independent Research Program
Work Unit A91-LD-003

Destroy this report when no longer needed. Do not return it to the originator.

The findings in this report are not to be construed as an official Department of the Army position unless so designated by other authorized documents.

The contents of this report are not to be used for advertising, publication, or promotional purposes. Citation of trade names does not constitute an official endorsement or approval of the use of such commercial products.

REPORT DOCUMENTATION PAGE

Form Approved
OMB No. 0704-0188

1. AGENCY USE ONLY (Leave blank)	2. REPORT DATE	3. REPORT TYPE AND DATES COVERED
	April 1992	Final report

4. TITLE AND SUBTITLE

Parameters Affecting Loads on Buried Structures Subjected to Localized Blast Effects

5. FUNDING NUMBERS

Work Unit A91-LD-003

6. AUTHOR(S)

James T. Baylot

7. PERFORMING ORGANIZATION NAME(S) AND ADDRESS(ES)

US Army Engineer Waterways Experiment Station,
Structures Laboratory,
3909 Halls Ferry Road, Vicksburg, MS 39180-6199

8. PERFORMING ORGANIZATION REPORT NUMBER

Technical Report SL-92-9

9. SPONSORING/MONITORING AGENCY NAME(S) AND ADDRESS(ES)

Department of the Army
Assistant Secretary of the Army (R&D)
Washington, DC 20315

10. SPONSORING/MONITORING AGENCY REPORT NUMBER

11. SUPPLEMENTARY NOTES

Available from National Technical Information Service, 5285 Port Royal Road, Springfield, VA 22161.

12a. DISTRIBUTION/AVAILABILITY STATEMENT

Approved for public release; distribution is unlimited.

12b. DISTRIBUTION CODE

13. ABSTRACT (Maximum 200 words)

Recent experiments have demonstrated that the current methodologies for predicting loads on buried structures resulting from the nearby detonation of a conventional weapon are not adequate. Errors in predicting the load could lead to significant errors in predicting the response of the structure.

In analyses which have been performed in the past to determine the response of structures to conventional weapons, decoupling assumptions were made so that the detonation of the charge in the soil is not included in the calculation. In these analyses assumptions are made which affect the loads applied to the structure. A procedure which did not require these types of assumptions was needed to determine the characteristics of the loads transferred to the structure. This required that the charge, soil, and structure be modeled in the calculation. Based on its user's manual, the finite element program DYNA3D had all of the characteristics needed to conduct this investigation.

After a preliminary review, it was determined that DYNA3D was not capable of performing these calculations without extensive modifications. These modifications included the implementation of a new Cap model for

(Continued)

14. SUBJECT TERMS		15. NUMBER OF PAGES
Buried structures	Ground shock	80
Conventional weapons	Loads on structures	16. PRICE CODE
Finite element analyses	Soil structure interaction	

17. SECURITY CLASSIFICATION OF REPORT	18. SECURITY CLASSIFICATION OF THIS PAGE	19. SECURITY CLASSIFICATION OF ABSTRACT	20. LIMITATION OF ABSTRACT
UNCLASSIFIED	UNCLASSIFIED		

13. (Concluded).

the soil. The new model was evaluated for its accuracy in reproducing free-field stresses for clay and sand, and can be used immediately adjacent to the explosive source. Due to large deformations and very high strains and strain rates in the soil near the charge, it was difficult to maintain the stability of the calculation. A method of maintaining this stability without adversely affecting the character of the free-field stress and velocity time-histories was developed and validated. A suitable method for simulating a nonreflecting boundary for soil responding inelastically was also developed. Calculations were performed for sand and clay soils to verify that DYNA3D with all of the modifications was capable of adequately predicting free-field stresses and velocities. These predictions agreed reasonably well with test data and indicated that the modified version of DYNA3D would be useful in investigating SSI. The nonreflecting boundary methodology was also verified.

One-dimensional cylindrical and spherical geometry assumptions were imposed and analyzed to determine if it was reasonable to perform the SSI study using a two-dimensional (2-D) plane strain model. These analyses indicated that a charge can be selected for the plane strain calculation so that the peak stress, maximum velocity, and stress and velocity gradients at the center of the structure match those which are predicted using the correct charge and a three-dimensional geometry. A 2-D model was selected to study SSI.

PREFACE

This report documents the analyses performed to develop a methodology for studying soil-structure interaction when a conventional weapon detonates near a buried hardened structure. The work was sponsored and funded through the In-House Laboratory Independent Research Program, work unit number A91-LD-003, work unit title, "Parameters Affecting Loads on Buried Structures Subjected to Localized Blast Effects."

These analyses were performed in the Structures Laboratory (SL), U.S. Army Engineer Waterways Experiment Station (WES), by Mr. James T. Baylot, Research Structural Engineer, Structural Mechanics Division (SMD), under the general supervision of Messrs. Bryant Mather and James T. Ballard, Director and Assistant Director, SL, respectively; and under the direct supervision of Drs. Jimmy P. Balsara, Chief, SMD, and Robert Hall, Chief, Analysis Group, SMD. This report was prepared by Mr. Baylot. Mr. Leonard I. Huskey is manager of the ILIR Program, and Ms. Mary K. Vincent, Chief, Office of Technical Programs and Plans, provides overall coordination for the program.

At the time of publication of this report, Director of WES was Dr. Robert W. Whalin. Commander and Deputy Director was COL Leonard G. Hassell, EN.

CONTENTS

CONVERSION FACTORS, NON-SI TO SI (METRIC) UNITS OF MEASUREMENT

Non-SI units of measurement used in this report can be converted to SI (metric) units as follows:

Multiply	By	To Obtain
feet	0.3048	metres
inches	25.4	millimetres
pounds (force)	4.47222	newtons
pounds (force) per square inch	0.006894757	megapascals
pounds (mass)	0.4535924	kilograms
pounds (mass) per cubic foot	16.01846	kilograms per cubic metre

Parameters Affecting Loads on Buried Structures Subjected to Localized Blast Effects

PART I: INTRODUCTION

Background

1. The military has many important facilities which must be capable of surviving a conventional weapons attack. Quite often these facilities are massive reinforced concrete rectangular structures in a buried configuration. These structures are extremely expensive to construct, and good design procedures are needed to provide an economical, yet safe design. Since these facilities will be located at sites throughout the world, there are many different types of backfill materials which may be used.

2. There are two options available to those responsible for designing these structures. They can import a favorable soil type, such as sand, to be used as the backfill material, or they can use the native soil. The cost of importing the sand is offset, at least partially, by the reduced structure cost. Once both designs are considered, the cheaper method can be selected. However, since there is less confidence in designing the structure in the other backfill types, the designer will often select importing the sand backfill material. This leads to structures that are much more expensive to build than they would have been if more reliable methods of assessing the importance of soil parameters were available.

3. Probably the most difficult phase of designing a buried structure to resist the effects of a conventional weapons detonation is the determination of the loads on the structure. Generally the free-field stresses (the stresses which would be present if the structure was absent) at the location of the point on the structure are computed. These stresses are modified to approximate the effects of the structure and its response. These modified stresses (interface stresses) are applied as the structure loading. Army Technical Manual (TM) 5-855-1 (U.S. Army Engineer Waterways Experiment Station 1986) provides one method of determining the loading from the free-field stresses. Another method has been proposed by Drake et al. (1987).

4. In TM 5-855-1, semiempirical methods to determine interface stresses from the free-field stresses are used. The method recommended by Drake uses continuity of velocities and stresses at the interface, along with linear-elastic, plane-wave theory to predict interface stresses. In this method the loading on the structure is predicted using the free-field stresses and velocities and the structure velocity. This method will be referred to as the structure-medium interaction (SMI) method. One more simplifying assumption which can be made is that the free-field stress is the acoustic impedance multiplied by the free-field velocity. Using this assumption, the free-field velocity time-history is not needed. This method will be referred to as the modified SMI (MSMI) method.

5. A series of tests (Baylot et al. 1985) has been conducted to study the parameters affecting the response of buried structures to conventional weapons effects. These tests were sponsored jointly by the Air Force Engineering and Services Center (AFESC) and the Office, Chief of Engineers, U.S. Army (OCE) and will be referred to as the AFESC tests. In the AFESC tests, eleven tests were conducted in a sand backfill material. The tests were designed to study the effects of span-to-thickness ratio and reinforcing-steel ratio of the slab and charge orientation and standoff distance.

6. Data from these tests were studied (Baylot and Hayes 1989) in great detail to evaluate the different methods of predicting interface stresses from free-field stresses and velocities. The methods presented in TM 5-855-1 of predicting interface-pressure loads from free-field stresses significantly overpredict the loading on the structure and, thus, structural response is significantly overpredicted. The SMI and MSMI methods appear to do a reasonable job of predicting the very early time-interface stresses, but may significantly underpredict later time loading. This later time loading can contribute significantly to the response of the structure, especially when deformations are large. For thinner slabs, these data indicate that some other method of predicting the later time loading is needed.

7. The Defense Nuclear Agency recently sponsored a series of conventional weapons backfill experiments (CONWEB) to study the effect of soil type on structure response (Hayes 1989). They showed that the soil type is extremely important in determining the loads on and, thus, the response of

buried structures. In a clay backfill experiment, the structure failed; while in an identical experiment in a sand backfill, minor damage was incurred.

8. These recent studies indicate that one current method of designing buried structures for conventional weapons threats may be overly conservative, while the other method may underpredict response. Neither method adequately predicts the differences in response caused by different backfill materials. Since the objective of the design is to provide the most economical design, which will provide the desired level of protection, neither method is completely satisfactory. For this reason, a study is needed to determine those parameters which significantly affect the response of buried structures.

9. Although much can be learned by conducting experiments on model structures and carefully examining the data, there are generally factors which complicate the interpretation of results and make the type of study needed impossible to perform with experimental data alone. One good approach for conducting this study is to perform calculations to model the experiments, and once these calculations are performed acceptably, this approach can be used to conduct parameter studies. The finite element (FE) method is an excellent tool for performing these analyses. The charge, soil, and structure can be modeled using the FE method so that assumptions about the SSI are not needed. After the calculations have been performed, the output may be studied to gain information on the characteristics of this SSI and the parameters that affect it. Both two- (2-D) and three- (3-D) dimensional calculations can be used.

10. FE calculations (Weidlinger and Hinman 1987) have been used to analyze buried structures subjected to conventional weapons effects. These analyses used equations from TM5-855-1 and procedures similar to those recommended by Drake, to determine the loads on the structure. Bogosian* used a "soil island" approach to analyze the wall of a buried structure. In this analysis, a small portion of the soil in front of the structure was modeled and stresses were input on the free boundary of the soil. The "soil island" method will be discussed more fully in a later section. Either of

* Presentation, 19 September 1989, Mr. David Bogosian, Karagozian & Case Structural Engineers, South Pasadena, CA, at "Conventional Weapons Backfill Test" meeting sponsored by the Defense Nuclear Agency, Alexandria, VA.

these methods uses assumptions which affect the loads transferred to the structure and are therefore not appropriate for the SSI study.

11. In order to perform the SSI analyses, the FE code must contain methods of modeling the explosives and the nonlinear behavior of the soil and the structure. The code should be capable of modeling the interface between the soil and structure and should have a nonreflecting boundary capability. The computer code, DYNA3D (Hallquist and Benson 1987), has these capabilities. DYNA3D is widely available at no cost to those interested in performing these type of analyses. This, coupled with the fact that this type of analysis has not been performed, indicates that using DYNA3D will probably be difficult, if not impossible. Before DYNA3D can be used to study SSI, it must be shown that DYNA3D can be used to successfully predict free-field, stress and velocity time-histories.

Objective

12. The objective of this study was to develop a computational procedure in which the detonation of the explosive, propagation of stresses through the soil, interaction of the soil with the structure, and structure response are modeled in a single analysis. Thus, assumptions are not needed to compute structure loads from free-field stresses. This procedure can then be used to study SSI.

Approach

13. Based on documentation in its user's manual, DYNA3D should be capable of performing the desired analyses if the Cap model used to model the soil can be modified to perform in the very high stress region adjacent to the explosive source. Before these modifications were made, calculations were performed to determine if the Cap model functioned well in regions of low stress for the clay material properties. This Cap model would not converge to a solution for the sample test case used, therefore, this Cap model was not suitable for modifications to make it perform well in the high stress regions. Pelessone (1989) had also determined that the Cap model in DYNA3D was not acceptable for calculations in soil materials and developed another version of

the Cap model which was acceptable. This Cap model was obtained, installed in DYNA3D, and modified so that it could be used in the very high stress region near the charge.

14. Once an acceptable Cap model was developed, DYNA3D was used to perform a series of calculations to determine if the free-field stresses and velocities could be adequately predicted for the CONWEB clay and sand backfill. One-dimensional (1-D) spherical calculations were performed by enforcing spherical boundary conditions. These calculations were unstable and a method of stabilizing the calculations without adversely affecting the predicted results was developed.

15. There are several parameters which must be determined in developing the FE model to be used in the SSI study. These parameters could affect the accuracy and stability of the solution as well as the time required to perform the calculations. Therefore, 1-D spherical calculations were performed to determine optimum values for parameters such as grid spacing, maximum strain increment, and critical time-step ratio.

16. The SSI investigation may be performed using a 2-D model of the explosive, soil, and structure. As far as the charge and free-field are concerned, this is a 1-D cylindrical geometry as opposed to the 1-D spherical geometry of the free-field if a 3-D model of the problem is used. Therefore, it was necessary to determine the effects of using cylindrical versus spherical boundary conditions.

17. Original calculations were performed with the boundary far enough away so that reflections did not come back to the points of interest during the time of interest. During the actual analyses performed to study SSI, a large number of nodes and elements will be needed to adequately model the explosive, soil, and structure. For these computations to be performed in a reasonable amount of time, the total number of nodes and elements must be limited. Since the coarseness of the grid affects the calculated results, it is desirable to reduce the number of nodes and elements by reducing the amount of soil being modeled. Therefore, it will be impossible to have boundaries that are far away, and a nonreflecting boundary must be used at the boundary.

Calculations were performed to assess the nonreflecting boundary used by DYNA3D. An error was found in this nonreflecting boundary. This error was corrected, however, the boundary still did not perform adequately. Modifications to the nonreflecting boundary were made.

PART II: MODELING CONSIDERATIONS

General Considerations

18. There are a number of important factors which must be considered if a useful SSI study is to be conducted. Typically, the structure will be designed for a relatively close-in detonation of the weapon. Since the weapon will be close in, damage will be localized and a higher level of damage is usually acceptable. Thus, the analysis must consider the closeness of the charge to the structure and the possibility of both geometric and material nonlinearities in the soil and structure responses. DYNA3D allows for both material and geometric nonlinearities.

Explosive Charge

19. The detonation of the charge must be included in the calculation. This can be done by directly including the detonation of the charge or by using a "soil island", where a portion of the soil is included in the calculation, and stresses and/or velocities are input at the free boundary of the soil. Thus, experimental data or results of previous calculations can be used to prescribe the stresses and/or velocities at the boundary. This free soil boundary must be taken between the charge and the structure.

20. This method is adequate as long as the time of interest in the calculation is small. Since the charge is close to the structure, the boundary along which stresses are input must also be close to the structure. When the stress wave propagating through the soil strikes the structure, a stress wave is reflected back into the soil. This wave will propagate back towards the boundary and will try to interact with the stresses and velocities at the boundary. Since these stresses and/or velocities are already specified, the interaction cannot occur, and artificial reflections will occur off of the boundary. The analysis is only valid until these reflections reach the structure again. Thus, it is desirable to directly include the charge in the calculation.

21. DYNA3D contains the Jones Wilkins Lee (JWL) equation of state model which can be used to model the explosive (Dobratz 1981). DYNA3D is capable of

modeling the propagation of the detonation through the explosive source, with the detonation starting from one or several points (lines or planes), or the calculation can be started after the explosive is completely detonated. A study* has been conducted to determine the differences between the two. This study showed that there was little difference, except for very close to charge, which is not of interest in this study. Therefore, this study was performed neglecting the effects of the propagation of the explosion through the source. Parameters input for this model are available (Dobratz 1981) for a number of different explosives types. The JWL parameters for C-4 as used in this study are listed below. The mass density is also listed below. The JWL equation of state is:

$$P = A[1-w/(R_1V)]e^{-R_1V} + B[1-w/(R_2V)]e^{-R_2V} + wE/V$$

where :

P	= Pressure, psi	
A	= Pressure coefficient	8.844×10^7 psi**
B	= Pressure coefficient	1.878×10^6 psi
R_1	= Coefficient	4.5
R_2	= Coefficient	1.4
w	= Coefficient	0.25
V	= Specific volume, ratio of current-to-original volume	
E	= Internal energy	psi-in.^{3}/in.^{3}
E_0	= Initial internal energy	1.305×10^6 psi in.^{3}/in.^{3}
ρ_o	= Original mass density	1.497×10^{-4} lb sec^2/in.^{4}

* Letter dated 11 May 1989, subject: "Analysis of Burn/No Burn Options for 1-D High-Explosive Spherical Source Calculation." From H. D. Zimmerman, California Research and Technology, Inc., Chattsworth, California, to Dr. J. G. Jackson, Chief, Geomechanics Division, Structures Laboratory, U.S. Army Engineer Waterways Experiment Station, Vicksburg, Mississippi.

** A table of factors for converting non-SI units of measurement to SI (metric) units is presented on page 3.

Soil Model

22. The nonlinear behavior of the soil between the charge and the structure must be modeled correctly. The Cap model is available in DYNA3D and is very suitable for modeling the nonlinear behavior of soils (Sandler and Rubin 1979) and (Simo et al. 1985). Therefore, it was selected to model both the clay and the sand experiments in the CONWEB test series. It was determined that this Cap model was not functioning correctly, and another Cap model was obtained (Pelessone 1989). The new Cap model is very similar to the one installed in DYNA3D. It was modified so that the model could be used in the very high pressure region adjacent to the explosive. The material properties for the Cap model were obtained from static uniaxial strain and triaxial compression test data; however, minor modifications were needed to make them perform correctly. These modifications will be discussed later in this report. Numerous parametric calculations were then made to determine the critical element size, critical time-step size, and artificial viscosity coefficients.

23. A complete description of this Cap model is provided in Pelessone (1989). A very brief summary will be presented here. This model uses soil mechanics sign conventions (compressive stresses and strains are positive). The Cap model is a two-invariant model where yielding is based on the square root of the second invariant, J_2', of the deviatoric stress tensor, given by:

$$J_2' = 1/2\ (s_{ij}s_{ij} + s_{ii}^2)]$$

where s_{ij} is the deviatoric stress tensor $s_{ij} = \sigma_{ij} - P$

σ_{ij} is the stress tensor

P is the pressure, $P = I_1/3.0$

I_1 is the first invariant of the stress tensor $I_1 = \sigma_{ii}$

and repeated subscripts imply summation.

J_2' is also given by:

$$J_2' = 1/6[(\sigma_{11}-\sigma_{22})^2+(\sigma_{22}-\sigma_{33})^2+(\sigma_{33}-\sigma_{11})^2]+ \tau_{12}^2+\tau_{23}^2+\tau_{13}^2$$

24. The yield surface is defined by the curve in Figure 1. Yielding occurs when $\sqrt{J_2'}$ reaches this envelope. This figure shows that the yield surface consists of three parts designated the tensile cutoff, the failure

surface and the Cap. The tensile cutoff is a constant, and the failure surface is a function of I_1, and is given by:

$$f = \alpha - \gamma \exp(-\beta I_1) + \theta I_1$$

where α, γ, β, and θ are material constants

f is the failure surface

25. The Cap is elliptical in shape and is movable. The intersections of the Cap with the failure surface and the I_1 axis, respectively, occur at L and X, as shown in Figure 1. X is determined from the volumetric plastic strain and the hardening function given below. L is determined from X and the aspect ratio, R, of the Cap. R is a material constant to be determined from test data. One difference between the new Cap and the one installed in DYNA3D is that a continuous function is used to describe the yield surface. Thus, there is no discontinuity in slope at L. The hardening function is shown in Figure 2 and is defined by:

$$e_v^p = W[1-\exp(-D1(X-X0)-D2(X-X0)^2)],$$

where e_v^p is the volumetric plastic strain.

W is the maximum volumetric plastic strain.

X is the current Cap location.

X0 is the initial location of the Cap.

W, D1, D2, and X0 are material constants, which must be determined. This is slightly different from the Cap installed in DYNA3D, which did not include the term including the constant, D2.

26. Associative flow rules are used to define the incremental plastic strains. Thus, the incremental plastic strains are normal to the failure surface. In this version of the Cap model, the elastic response of the material is defined by constant bulk, K, and shear, G, moduli. At very high pressures, the bulk modulus increases significantly. For the material very close to the charge this increase must be modeled. The Cap model was modified to include the following function for the elastic bulk modulus:

$$K = K_I + K_1 P^{K2}$$

where K is the bulk modulus

K_I, K_1, and K_2 are material constants.

27. In DYNA3D the function of the constitutive model is to return the next stress state given the current stress state and a strain increment. The stress-strain response during this strain increment may be highly nonlinear. Some procedure must be used to ensure that stresses outside the yield surface are not predicted, and that plastic flow is normal to the yield surface. In the original Cap model, an iterative procedure was used. In the new Cap model the strain increment was subdivided into a large number of smaller increments within the constitutive model. The critical strain increment is given by:

deltep = 0.05 (α - γ) [minimum of (1./G and R/9K)]

For the clay material tested in the CONWEB series, this equation implies that a strain increment of 1.39×10^{-8} must be used. Since very large strains are expected in the soil near the charge, an extremely large number of strain increments will be needed. For a large grid such as the one to be used for the SSI analyses, using a maximum strain increment of this size would drastically increase run times. Therefore, the Cap model was changed so that the maximum strain increment is now a user input. The strain increment that will be needed will, in general, depend on the material properties selected and the stress state to which the material is subjected. Parametric analyses were performed to determine the optimum maximum strain increment for the sand and clay materials.

Artificial Viscosity Coefficients

28. Two other inputs into the FE model are the viscosity coefficients. Linear and quadratic viscosity coefficients are input into the code to stabilize the calculation. In most FE calculations, the default values of these coefficients are appropriate. They are large enough to stabililze the calculation but are small enough so they do not adversely affect the results of the calculation. These coefficients are transparent to the typical FE code user who probably does not know that they are there. The viscosities are used to generate artificial forces that are proportional to the volumetric strain rate and the square of the volumetric strain rate, respectively. The quadratic viscosity is only active during the original loading of the material. These coefficients affect the character of the results, as well as the stability of the solution. In general, the smallest amount of viscosity

which will stabilize the solution should be used. Analyses are needed to determine the appropriate viscosity coefficients to be used in the SSI study.

Grid Size

29. The solution will also be affected by grid parameters such as element dimensions and location and types of boundaries used. Test data have shown that the rise times associated with stresses at a point in the soil near a conventional weapons detonation are very small, much smaller than the natural period of the structure wall. Since this rise time could affect the response of the structure, it is important that the rise time is as close to correct as is possible. In the calculation, the rise time is affected by the material properties as well as the grid spacing. The SSI analyses require that a large area be modeled. Thus, the grid spacing should be optimized. Analyses were performed to determine the maximum grid spacing, which adequately predicted the rise times on free-field stresses.

30. In the test events, the soil around the structure continued for a great distance. This amount of soil cannot be modeled in the FE analysis. The FE grid must be stopped, and some type of boundary conditions enforced at the boundary. There are several types of boundaries that have been used to model a nonreflecting boundary (Lysmer and Kuhlemeyer 1969) and (Underwood and Geers 1978). This boundary simulates an infinite amount of soil placed behind it. This boundary has been shown to be very effective in modeling material responding in the elastic range (Underwood and Geers 1978) but did not perform well when modeling the nonlinear behavior of soils (Underwood and Geers 1979). A nonreflecting boundary is available in DYNA3D, and this boundary could be very useful if it could be shown to be effective. Therefore, analyses were performed to assess this nonreflecting boundary.

Time Step

31. Since DYNA3D is an explicit FE code, the time step selected is critical to the calculation. DYNA3D selects a critical time step for each element based on the dimensions and wave speed in that element. The critical time step is the smallest time step determined for any of the elements. The

wave speed is computed based on constant elastic material properties and does not consider that these properties may change with stress level. Therefore, it is possible that the critical time step selected is not small enough. A scale factor to reduce the critical time step can be input into DYNA3D. Analyses were performed to determine the optimum critical time-step factor.

Two-Dimensional Effects

32. In the test event, a cylindrical charge was placed relatively close to the test structure. The 27-in.-long charge was placed 60 in. from the structure. It has been shown that the free-field stresses and velocities in clay and sand, respectively, can be predicted reasonably well using a spherical charge and assuming spherical symmetry (Zimmerman et al. June 1990) and (Zimmerman et al. October 1990). Many of the SSI analyses will be performed on a 2-D model. In effect, the charge will be an infinitely long cylinder. The stresses in this case will attenuate in a 2-D space rather than a 3-D space, and the effects of this difference should be investigated. Analyses using 1-D cylindrical and spherical boundary conditions were performed in the sand and clay materials to assess the importance of this difference.

PART III: PARAMETER STUDIES

Material Models

33. Constants for the modified Cap model have been determined for the CONWEB clay* and sand.** These constants are based on static tests of those materials. These constants (Table 1) were obtained by using a constitutive model driver to simulate static tests which had been conducted on the two materials.

34. Since the Cap parameters are determined using static tests of recompacted material, some modifications may be needed to make the response match that of the material tested in the model tests. Nelson† determined that the material in the CONWEB clay test was stiffer than was indicated by the laboratory tests, and found that if the hardening parameter, D1, was decreased to 0.0004/psi, the calculations would do a better job of matching data. Therefore in the clay calculations, a D1 value of 0.0004 was used instead of that determined from laboratory tests. The material properties using this value of D1 will be referred to as the modified material properties for clay. A comparison of the volumetric stress-strain curves using the two different values of D1 is given in Figure 3. All other parameters were as determined in the laboratory tests. No previous analyses were available for the sand material; therefore, the appropriate material constants had to be determined by performing analyses and comparing them to test data.

---

* Personal Communication, 1 November 1989, Dr. Jon Windham, Research Civil Engineer, U.S. Army Engineer Waterways Experiment Station, Vicksburg, Mississippi.

** Personal Communication, 14 August 1990, Mr. Steve Akers, Research Civil Engineer, U.S. Army Engineer Waterways Experiment Station, Vicksburg, Mississippi.

† Letter, 13 March 1990, from Dr. Ivan Nelson, Weidlinger Associates, Inc., Consulting Engineers, New York, New York, to Dr. Jon Windham, Research Civil Engineer, U.S. Army Engineer Waterways Experiment Station, Vicksburg, Mississippi.

Spherical Clay Analyses

35. Analyses to determine optimum values of the FE parameters for the SSI calculation can be performed much more efficiently using a 1-D spherical grid as opposed to using a full 3-D grid, which would give the same results. Therefore the grid shown in Figure 4 was used. This grid was one element thick in the y and z directions, and the x direction represented the radial direction of the spherical calculation. In order to simulate the spherical runs, the y and z dimensions of the elements must increase in proportion to the x distance of the element from the origin. In most of the calculations a 6-degree sector of a sphere was used. Boundary conditions were specified such that the nodes must slide along radial lines passing through the origin, since this must be the case for spherical symmetry. Each of the elements representing the soil was an 8-node solid element. Since the charge was located at the origin, the four nodes located at a radius of 0.0 in. collapsed to one node, leaving a five node solid. The DYNA3D user's manual (Hallquist and Benson 1987) shows that only 4-, 6-, and 8-node elements are available to model solids; therefore, the element was divided into two 4-node elements, as shown in Figure 5.

36. It was desired to compare the results of these analyses to measured test data to determine if the FE code predicts free-field stresses and velocities that are realistic. Test measurements were made at 3, 4, 5, 6, and 7 ft away from the charge, and 20 msec was selected as the time of interest. Therefore, the grid was made large enough so that reflections from artificial boundaries, such as the end of the grid, did not reach the test-gage locations within 20 msec. In most of the analyses performed, the soil boundary was placed at 40 ft from the center of the charge.

37. In the CONWEB experiments, a controlled backfill was placed in a finite test pit around the structure. The charge was buried to a depth of 5 ft below the ground surface. The test pit boundaries and the free surface at the top of the backfill affected the stresses and velocities measured in these experiments. These effects were not considered in the analyses, and this affects comparisons with the data.

38. Typically in performing FE calculations, an attempt is made to develop a grid containing elements with aspect ratios close to 1.0. Since the y and z dimensions of this grid are growing with the distance of the element from the origin, the x dimension of the element must also grow with distance from the origin. In order for the first soil element to have aspect ratios of 1.0, the x dimension of the first element must be approximately the charge radius, 4 in. times sin(6), 0.4 in. In order to maintain this aspect ratio, the x dimension of the elements must grow by a factor of 1+sin(6). Using this size element near the charge and this growth rate will produce an element at the 5-ft range, which has an x dimension of approximately 6 in.

39. If a 2-degree sector was used instead of a 6-degree sector an x dimension of approximately 2 in. would be produced at the 5-ft range. However, this would greatly increase the number of elements needed for the SSI calculations. Therefore, the effect of using elements with variable aspect ratios, not necessarily close to one, was investigated. Calculations were performed with elements using a constant spacing in the x direction and compared to those with a constant aspect ratio of approximately 1.0. Calculations were also performed to determine the optimum constant spacing. The charge in the tests was a cylindrical charge, encased in steel, containing 15.4 lb of C-4. A sphere containing the same weight of C-4 has a radius of 4 in. Therefore, analyses were performed using a 4-in.-radius sphere.

40. In those analyses where the time step was too large or the maximum strain increment or viscosity coefficients were too low, the solution was unstable and the stress time-histories near the charge look similar to the one shown in Figure 6. Stable solutions could not be obtained using the default values for the artificial viscosity coefficients. In some cases the stress time-histories further away appeared to be acceptable. Even if the stresses further away from the charge appear to be acceptable, the parameters associated with these analyses were rejected because the effects of the instability near the charge cannot be evaluated and run times increased drastically due to the instability. Once a stable solution was obtained, further parametric calculations were performed to assess the accuracy of the solution.

41. Figure 7 shows a comparison of the results of computations using a constant aspect ratio of approximately 1 to the results of a computation using a constant element thickness of 1 in. A complete description of these computations is provided in Table 2. These are the 6- and 2-degree constant aspect ratio computations described above. In the constant aspect ratio computation, the elements are thinner near the charge than in the constant thickness analyses. This results in higher stresses in the elements near the charge and higher viscosities, and smaller strain increments are required. Figure 7 shows that the rise times are much faster in the constant thickness computation. This is because near the points of interest, the elements are much larger in the constant aspect ratio computation, and the rise time is clearly a function of the element thickness. The rise time also increases in the constant aspect ratio analyses using the variable radial spacing because of the increased artificial viscosity required in these runs. Rise times could be improved by taking a larger number of elements in the constant aspect ratio analysis, but this would make the elements near the charge extremely small, and since the critical time-step is based on wave travel time across an element, this would increase computation time considerably. The rise times associated with the constant thickness elements more nearly match those of the test data, and the constant thickness element was selected for the remaining calculations.

42. The results of one of the analyses are compared with experimental data in Figures 8 and 9. Gage locations were 3, 4, 5, 6, and 7 ft from the charge with the stresses (velocities) arriving at the gages in order, based on distance from the charge. In this analysis, the modified Cap parameters were used. The viscosities were five times the default viscosities. A maximum strain increment of 0.0001 and a time-step of 0.1 times the computed critical time-step were used. The grid consisted of 1-in. elements up to 40 ft away from the center of the charge. These figures show that, qualitatively, the results compare very well with the data. However, the computed peak stresses and velocities were much lower than the measured values.

43. Since, qualitatively, the results were good, it appears that the type of constitutive model being used was acceptable. A number of parametric calculations were then performed in an attempt to tune the material properties so that a better match of peak stresses and velocities with the data could be

obtained. The failure surface of this material is very low, and essentially all of the response will be in the plastic range. Unless the failure surface is modified drastically, the change will be insignificant. Therefore, changes to the failure surface were not made. The bulk modulus and hardening function parameters were varied to determine their effect on the stress and velocity time-histories. These runs showed that changes in the material properties could raise the stress levels to close to the measured values (Figure 10), but the peak velocities (Figure 11) changed very little. Figures 10 and 11 are the stress and velocity time-histories, respectively, at 5 ft from the charge. In this analysis, the same parameters used in the previous analysis were used, except for the maximum volumetric plastic strain, W, of 0.003, and the hardening function parameter, D1, of 0.00138.

44. These analyses indicated that changes in material properties had very little effect on the peak velocities. Since the characters of the stress and velocity time-histories were a good match to the data, it appears that the stress wave was propagating through the soil correctly, but that more energy was needed from the explosive source. It appears that the JWL model is not functioning correctly. This will be discussed more fully later in this report.

45. The purpose of this study is to examine the effects of soil parameters on the SSI, not to predict stresses and velocities in the free field. The amount of energy contributed by the charge can be increased by simply increasing the amount of charge in the analysis. Therefore, analyses were performed using the modified Cap parameters for various charge sizes. Calculations were performed for 5-, 6-, 7-, 8-, and 9-in. radius charges. It appears that a charge radius between 6 and 7 in. is needed. Therefore, analyses were performed using 6- and 7-in. radius charges to determine the maximum strain increment, critical time-step factor, and optimum grid spacing.

46. Preliminary calculations using the constitutive driver indicated that at a maximum strain increment above 0.0001, the model becomes unstable. Therefore, this was the highest maximum strain increment considered. The DYNA3D user's manual recommends that the critical time-step factor be taken as 0.67 when explosives are being modeled. Therefore, this is the largest time-step scale factor considered. Calculations were performed at grid spacings of 0.5, 1.0, and 2.0 in.

47. Figures 12 and 13 compare the stress and velocity time-histories, respectively, at a range of 5 ft from the charge for calculations using 1/2- and 1-in. grid spacings. Experimental data are also included for comparison. These figures show that the rise times at this range are modeled well by either the 1-in. or the 1/2-in. grid. It appears that the 1-in. grid spacing will be adequate since there is very little difference in the results of these two runs. A comparison between the results using a 2-in. grid spacing and those using a 1/2-in. spacing is shown in Figure 14. This figure shows that the rise time is significantly different when the 2-in. grid spacing is used. Therefore, a 1-in. grid spacing was selected to be used in further calculations.

48. In order to determine the importance of the critical time step factor, two computations were performed. Time-steps of 0.1 and 0.67 times the critical time-step were used. Radial stress and velocity time-histories at the five different ranges were compared, and the results of the two computations were identical; therefore, it was concluded that a critical time-step factor of 0.67 was satisfactory.

49. Parametric calculations were performed for maximum strain increments of 0.00001, 0.00002, 0.00005, and 0.0001. The computations using the 0.0001 increment were unstable. The radial stress time-histories at the 3-ft range for the other three analyses are compared in Figure 15. This figure shows that the results were identical for the 0.00001 and 0.00002 strain increments, while the arrival time was slightly greater and the peak stress was less for the analysis using the 0.00005 strain increment. The decays of the stress time-histories were approximately the same for all three analyses. Figure 16 shows the same comparison for a range of 5 ft from the charge. This figure also shows exact agreement between the computations using strain increments of 0.00001 and 0.00002. The agreement of the computations using the 0.00005 strain increment with the other analyses was much better at this range. The arrival was only slightly later, and the rise time and peak stresses were very nearly the same. In the SSI analyses, the structure will be placed at 5 ft from the charge. Since the stress time-history predicted using a maximum strain increment of 0.00005 is very nearly identical to those predicted using smaller strain increments, this strain increment should be acceptable for performing the SSI study.

50. The results of one FE analysis are compared to test data in Figures 17 and 18. In this analysis a 6-in. charge, 1-in. grid spacing, 5 times the default viscosities, a critical time-step factor of 0.67, and a maximum strain increment of 0.00005 were used. Figure 17 shows that analysis results compare extremely well with the stress time-histories at the 3- and 4-ft ranges, but stresses were over predicted at the other ranges. At the 5-, 6-, and 7-ft ranges, the computed rise times were slightly greater and the stresses decay slower than those measured in the test. The arrival times of the peak stresses were predicted reasonably well at all ranges.

51. Figure 18 shows that the velocity time-histories at the 3- and 4-ft ranges were predicted well. At the 5-, 6-, and 7-ft ranges the velocities are overpredicted. Rise times were predicted reasonably well at all ranges, but arrival times are different from the data at each of the ranges. The arrival time, based on velocity at a given range, should be the same as the arrival time based on stress for that range. This is true based on the analysis, but is not true based on the data. This is probably due to the methods used for collecting the velocity and stress data.

52. These analyses required that relatively high artificial viscosities be used. These high viscosities cause the rise times of the stress and velocity time-histories to increase with distance from the charge, and these rise times were too long as compared to test data. Analyses were performed to determine if using artificial viscosity coefficients that varied with distance from the charge would improve the rise times at the ranges farther away from the charge. An analysis identical to the one shown previously was performed, except that the maximum strain increment was 0.00002, and variable artificial viscosity terms were used. When variable artificial viscosities were used, there was a significant difference between the computation using a maximum strain increment of 0.00002 and the one using 0.00005. Therefore, 0.00002 was selected. In this analysis, the following multiples of the default viscosities were used:

Range from charge, in.	Multiple of default viscosities
R < 42	5
42 < R < 48	4
48 < R < 60	3
60 < R < 72	2
72 < R	1

53. Figure 19 compares the results of this analysis with the previous analysis and test data. There were no differences between the stress or velocity time-histories for these two analyses at the 3- and 4-ft ranges; therefore, those ranges are not shown. At the 5-ft range, there was a slight improvement in the rise time. At the 6- and 7-ft ranges, there was a significant improvement in both rise times and arrival times. Figure 20 shows that the arrival times of the velocities did not agree as well with the velocity data, but the rise times using the variable viscosities agreed better with the data at the 5-, 6-, and 7-ft ranges. These analyses showed that using artificial viscosities, which vary with range, can significantly improve the rise times of the stress and velocity time-histories. The use of these variable viscosities will produce stress and velocity time-histories which are more like those measured in the test.

Cylindrical Clay Analyses

54. Since a 2-D grid may be used for many of the SSI studies, the effects of using a cylindrical geometry as opposed to a spherical geometry should be investigated. It is desirable that the correct stress and velocity time-histories be predicted at least at the structure location. Therefore, the objective of these analyses is to determine if a charge size can be selected so that the correct stress and velocity time-histories are predicted at the structure location. Since the stress and velocity gradients at the structure will probably affect the SSI problem, the effect of the 2-D geometry on stress gradients should also be investigated. Ideally, near the structure

the attenuation of peak stress (velocity) versus range should be the same in order for the stress (velocity) gradients to be approximately the same.

55. FE analyses were performed using a cylindrical charge with a 1-in. radius. The computations were performed using a 1-D grid similar to the one used for the spherical analyses. In this case, the elements were 1-in. thick in the z direction and grew in the y direction as x increased. A 6-degree sector of a cylinder was used for these calculations, and boundary conditions were used to enforce cylindrical symmetry. Material properties were the same as those used for the spherical calculations. In these analyses, a critical time-step factor of 0.25 and a maximum strain increment of 0.00002 were used. The artificial viscosity factors were as follows:

Range from charge, in.	Multiple of default viscosities
$R < 6$	20
$6 < R < 12$	15
$12 < R < 24$	10
$24 < R < 36$	8
$36 < R < 48$	5
$48 < R$	3

56. Figure 21 shows that the stresses at the 5-ft location in the cylindrical analysis agree very well with those of the spherical analysis. Figure 22 shows that the maximum velocities agree reasonably well between the two analyses, but the velocities decay slightly faster for the cylindrical analyses. Peak stresses versus range from the charge are shown in Figure 23. This figure shows that near the 5-ft range the stresses in the cylindrical analyses attenuate with range similarly to those in the spherical analysis, and both analyses match the data reasonably well. Figure 24 shows the attenuation of maximum velocity with range. This figure shows that the cylindrical analysis predicts the attenuation of maximum velocity with range reasonably well. These figures indicate that it is reasonable to use a 2-D model to perform the SSI studies.

57. Since artificial boundaries must be introduced into the SSI analysis, it is important to determine how well the nonreflecting boundaries work. In preliminary studies to evaluate the nonreflecting boundaries, it was discovered that the nonreflecting boundary was not affected by changing the properties of the material near the boundary. In investigating this problem

it was determined that the subroutine which passes material property information to the nonreflecting boundary subroutine was not passing the correct information. This was corrected and further studies were performed. Figures 25 and 26 show the effects of different boundary conditions on stresses and velocities, respectively, at 5 ft from the charge. The solid lines in these figures are for a nonreflecting boundary at 40 ft. This boundary was far enough away so that boundary effects did not appear for the time shown in these figures. The other results are for various types of boundaries placed at 10 ft from the charge. These figures show that the stresses and velocities based on the nonreflecting boundary at 10 ft were very close to those using the fixed boundary. This is not satisfactory for the SSI study.

58. The nonreflecting boundary is designed to simulate an infinite amount of material beyond the boundary. In DYNA3D the model is based on constant values of the shear and bulk moduli, and is, thus, only accurate if the boundary is placed in a region such that the soil is elastic. This is not true in this case, and the error introduced is obviously significant. Figure 27 shows a comparison of several forms of the volumetric stress-strain curve for this soil. Clearly, using the elastic constants only will produce a boundary that is much stiffer than it should be. The material model was modified so that the shear and bulk moduli used by the nonreflecting boundary subroutine could be different from those used by the constitutive model for those elements.

59. The volumetric stress-strain curve needed to tune the nonreflecting boundary is shown in Figure 27. This shows that the elastic constants must be selected so that the elastic stress-strain curve for the boundary matches the total stress-strain curve for the material. The elastic bulk and shear moduli were each divided by 80 in this case.

60. Figures 28 and 29 show comparisons of stress and velocity time-histories, respectively, based on analyses using the modified nonreflecting boundary at 10 ft from the charge, to those in which the boundary is too far away to be significant. These figures show that the modified boundary simulates a nonreflecting boundary very well.

Spherical Sand Analyses

61. The material properties of sand are significantly different from those of clay. Figure 30 shows that the failure surface of clay is almost constant and is much lower than that of sand. The failure surface in sand increases significantly with increasing mean normal stress. Figure 31 shows a comparison of the volumetric stress-strain curves for the clay and sand tested in the CONWEB test series. This shows that the stress-strain curve of the clay locks up at approximately 4 percent, while that of the sand locks up at approximately 26 percent. These numbers correspond to the percentage of the volume of each material which is initially filled with air, and indicate that once these air voids are closed further plastic volumetric straining does not occur.

62. One-dimensional spherical analyses similar to those performed for the clay material were performed for the sand material. Material properties for the Cap model for the sand were based on static tests. These material properties are listed in Table 1. As was the case with the clay, parametric calculations were performed to determine the required grid spacing, critical time-step ratio, artificial viscosity terms, and maximum strain increment.

63. In order to obtain suitable results, the value of the shape parameter D1 of the hardening function was changed from 0.0000758 per psi to 0.00003 per psi. All other material properties were as listed in Table 1. The material properties using this value of D1 will be referred to as the modified properties for sand. The effect of this change in D1 on the volumetric stress-strain curve is shown in Figure 31. The following parameters were needed to reasonably predict the stresses and strains in the sand test:

Charge Radius	6 in.
Grid Spacing	1 in.
Time-Step Ratio	0.67
Artificial Viscosity Terms	3 times default
Maximum Strain Increment	0.00001

64. Figures 32 and 33 compare the stresses and velocities, respectively, from this analysis with the test data. The computed arrival time of the stresses at 3 ft did not agree with the data; therefore, 0.3 msec

was subtracted from all of the data records to account for this difference. Figure 32 shows that stresses were predicted reasonably well for this test. In general, the arrival times were sooner in the calculation, and the rise times were longer. The arrival times become progressively worse with distance from the charge. For those measurements at 3, 4 and 5 ft, the analysis predicted that the stresses will drop more quickly from their peak values than was measured in the test. Late-time stresses were significantly overpredicted at all ranges as shown.

65. Figure 33 shows that the comparison of measured to computed free-field velocities is similar to the comparison of stresses. In general, the predicted maximum velocities agreed well with the test data. The predicted arrival times were too soon, and the rise times were too long. Unfortunately two of the gages (4 and 5 ft) malfunctioned after peak velocity was obtained, and complete velocity time-histories were not available. The data for the 7-ft range are not consistent with the remainder of the velocity data for this test, and this comparison with the test data cannot be made. For the other two gages, late-time free-field velocities were underpredicted . This is consistent with the overprediction of late-time free-field stresses and indicates that the free surface, which was not considered in the analysis, affected both late-time stresses and velocities in the experiment in sand. The relatively small and shallow test bed of sand was also surrounded by the native clay backfill material, similar to the clay previously analyzed. This effect, which was not modeled in the analysis, would also affect late-time stresses and velocities.

66. Further analyses were performed using artificial viscosity terms which varied with distance from the charge to determine if rise times and arrival times would be improved. The following multiples of the artificial viscosity terms were used:

Range from charge center, in.	Multiple of default viscosities
$R < 9$	3
$9 < R < 13$	2
$13 < R < 18$	1
$18 < R < 24$	0.5
$24 < R$	0.25

67. Figure 34 shows that arrival times and rise times of free-field stresses were significantly improved at all ranges when variable artificial viscosities were used. The histories were shifted so that the peak stresses at 3 ft would occur at the same time for the two analyses and the data. The peak stresses were increased slightly in the analysis using the variable artificial viscosities; and since the peak stresses were already slightly high, the agreement between predicted and measured peak stresses was worsened. Agreement with late-time stresses was not changed at all. Since the arrival and rise times were significantly improved with only a small increase in error in peak stresses, the overall effect of using the variable artificial viscosities was to improve the agreement between the predicted and measured stress time-histories.

68. The effect of variable artificial viscosity on free-field velocities is shown in Figure 35. Arrival times and rise times were both significantly improved by using the variable artificial viscosity. Maximum predicted free-field velocities were higher for the variable viscosity calculation, and agreement with the data was slightly worsened. The overall effect of using the variable artificial viscosities was to improve the agreement of the computed velocity time-histories with the test data.

Cylindrical Sand Analyses

69. Analyses were performed to determine the effects of using cylindrical versus spherical boundary conditions in the sand backfill material. A 1-in. radius charge was used in this study. Parametric calculations were performed until a good combination of the critical time step, maximum strain increment, and artificial viscosity terms was determined. The analyses were performed using the same grid as that used for the cylindrical analyses in clay. The material properties were the same as those used for the spherical sand analyses. In the cylindrical sand analyses, a critical time-step factor of 0.25 and a maximum strain increment of 0.00001 were needed. The following multiples of the default artificial viscosity terms were used:

Radius from center of charge, in.	Multiple of default viscosity
R < 3	30
3 < R < 5	20
5 < R < 9	10
9 < R < 16	5
16 < R < 24	3
24 < R < 46	2
46 < R	1

70. Figures 36 and 37 show comparisons between the analyses using cylindrical versus spherical boundary conditions for stress and velocity time-histories, respectively, for a range of 5 ft from the center of the charge. These figures show that the 1-in. charge did a good job of matching the stress and velocity time-histories at a range of 5 ft. Both stresses and velocities were slightly low, indicating that there probably is a slightly larger charge that would do a better job of matching the peak stresses and velocities. However, this analysis does indicate that an analysis imposing cylindrical boundary condition can be used to match the stress and velocity time-histories at the 5-ft range from a spherical source.

71. Figures 38 and 39 show the attenuations versus range of peak stress and maximum velocity, respectively, for the spherical and cylindrical geometries. These figures show that the attenuations versus range of peak stress and maximum velocity of the cylindrical analysis match those of the spherical analysis reasonably well near the 5-ft range. Either analysis matches the data reasonably well. Based on Figures 36-39 it is reasonable to use a 2-D model to study SSI in the sand material.

72. Figures 40 and 41 show the comparison of stresses and velocities, respectively, at the 5-ft range from the charge, between an analysis with the boundary far away, and another analysis in which a modified nonreflecting boundary was placed at 10 ft from the charge. The boundary was modified by dividing the elastic bulk and shear moduli, respectively, by 50. Figures 40 and 41 show that the modified nonreflecting boundary did an excellent job for at least 20 msec.

Charge Size

73. It was noted in a previous section that the charge size needed in the spherical calculations to match the data from the CONWEB experiments was a 6-in.-radius charge, while the charge used in the experiment was equivalent to a 4-in.-radius charge. Although it was not necessary for this study, it was desirable to understand the reason for this discrepancy.

74. In these analyses, two tetrahedral elements were used to model the explosive. In an effort to determine the source of this error, it was discovered that the volume of the tetrahedrons used to model the explosives was computed incorrectly. The source of this error is discussed in Appendix A. This error does not significantly affect the JWL model, but does significantly affect the nodal loads computed based on the pressure in the element. For the 6-in.-radius charge a volume of 0.29 cu in. was computed, while the actual volume was approximately 0.78 cu in.

75. If a very small portion of the volume is deleted from the center of the sphere, the sphere can be modeled using an 8-node solid element. Although this element has an extremely bad aspect ratio (approximately 20 based on the small dimension near the center of the element), the computed volume is very nearly correct. Analyses were performed for the sand material using a 4-in.-radius charge with 0.2 in. removed from the center. Thus, the charge can be modeled using a single 8-node element, and the volume is computed very nearly correctly (14 percent low). In these analyses, the modified sand properties were used. The critical time-step factor, artificial viscosity factor, and maximum strain increment were 0.67, 20, and 0.00001, respectively. The artificial viscosity factor was dropped to 5 at a distance of 12 in. from the center of the charge.

76. Figures 42 and 43 compare the stress and velocity time-histories, respectively, from this analysis to the test data. These figures show that the stress and velocity time-histories compare reasonably well with the test data. This indicates that a 6-in.-radius charge was needed in the analysis using the tetrahedral elements for the charge because the volume of the charge was computed incorrectly, and that more care should be taken in developing the grid for the explosives. The volume of the 6-node element used in the cylindrical calculations was computed correctly by DYNA3D.

PART IV: SUMMARY AND CONCLUSIONS

Summary

77. FE analyses which include the detonation of the explosive charge, propagation of stresses through the soil to the structure, interaction of the soil with the structure, and response of the structure are needed to study SSI. DYNA3D can model the detonation of the explosive using the JWL equation of state. It also contains a version of the Cap model, which has been demonstrated to be very effective for modeling wave propagation through soil materials. Subroutines in the code are available for modeling the interaction of the soil with the structure, and material and geometric nonlinearities can be analyzed. Therefore, DYNA3D appears to be ideal for investigative SSI. DYNA3D is widely available to engineers who would like to perform these calculations, and prior to this study there were no published reports of SSI analyses of this type using DYNA3D or any other FE code. It was therefore assumed that using DYNA3D for the SSI investigation will be difficult, if not impossible. This study was performed to determine if the detonation of the explosive and propagation of the stress wave through the soil could be adequately modeled.

78. Preliminary analyses showed that the Cap model in DYNA3D would not function for the material properties to be used in this study. Another Cap model was obtained and installed in DYNA3D. This Cap model uses a constant bulk modulus. This is adequate for the soil types being analyzed as long as pressures are not extremely high. However, at locations near the charge a bulk modulus which increases with increasing pressure is needed. The newly installed Cap model was modified to use a bulk modulus which increases with increasing pressure. This Cap model was also modified so that the maximum strain increment is input instead of being computed by the code. This made the Cap model much more efficient.

79. One-dimensional spherical calculations for comparison to the CONWEB clay and sand tests were then attempted. In these calculations, the DYNA3D default values of the viscosity coefficients were used and the runs were unstable. It was determined that much higher viscosity coefficients were needed to stabilize the results. However, when these large viscosities were

used, the rise times at locations away from the charge were much too high. When viscosity coefficients which decreased with increasing distance from the charge were used, the calculations were stable and the rise times were acceptable.

80. In addition, optimum values of grid spacing, maximum strain increment, and critical time step for the sand and clay materials were investigated. The results of these analyses compared reasonably well with experimental data.

81. In order to determine if the SSI study could be conducted in 2-D, one-dimensional cylindrical calculations were performed and compared to the 1-D spherical calculations. At the range of the structure, the same peak stresses and velocities as predicted for the spherical calculations could be obtained by using a cylindrical geometry and a smaller charge radius. The shapes of the stress and velocity time-histories at 5 ft were also reasonably close to those of the spherical calculations. At the structure range, peak stress and maximum velocity gradients in the cylindrical calculation also agreed very well with the spherical calculation.

82. The properties needed for the nonreflecting boundary subroutine were not being passed to that subroutine. This was corrected, however, the nonreflecting boundary was still much too stiff since the routine is based on the elastic bulk and shear moduli and is, therefore, too stiff if a nonreflecting boundary is placed in an inelastic region. The subroutine was modified so that a fraction of the elastic properties could be used. It was demonstrated that if the correct fraction of the elastic material properties is used, the nonreflecting boundary method in DYNA3D does a good job of simulating the continuum beyond the boundary. Factors for a boundary at 10 ft from the charge were determined for the clay and sand materials.

Conclusions

83. The Cap model in DYNA3D did not function correctly for the sand and clay backfill materials used in the CONWEB experiments. Stable solutions could not be obtained using the default viscosities and the nonreflecting boundaries in DYNA3D. Therefore, the unaltered version of DYNA3D could not be used to investigate SSI. The new Cap model did function well for the clay and

sand backfills and when it was modified to use a variable bulk modulus it could be used to model the soil adjacent to the charge. The modified nonreflecting boundary worked extremely well. DYNA3D using the modified Cap model, variable artificial viscosities, and the modified nonreflecting boundary is very suitable for performing the SSI study. It was also determined that the SSI study could be conducted in 2-D.

REFERENCES

Baylot, J. T., and Hayes, P. G. 1989 (Nov). "Ground Shock Loads on Buried Structures," Proceedings of the 60th Shock and Vibration Symposium, David Taylor Research Center, Bethesda, MD, Vol I, pp 331-347.

Baylot, J. T., Kiger, S. A., Marchand, K. A., and Painter, J. T. 1985 (Nov). "Response of Buried Structures to Earth Penetrating Conventional Weapons," ESL-TR-85-09, Air Force Engineering and Services Laboratory, Air Force Engineering and Services Center, Tyndall Air Force Base, FL.

Dobratz, B. M. 1981. "LLNL Explosives Handbook, Properties of Chemical Explosives and Explosive Simulants," Report UCRL-52997, Lawrence Livermore National Laboratory, University of California, Berkeley, CA.

Drake, J. L., Frank, R. A., and Rochefort, M. A. 1987 (Mar). "A Simplified Method for the Prediction of the Ground Shock Loads on Buried Structures," Proceedings of the International Symposium on the Interaction of Conventional Weapons with Structures, Federal Minister of Defense, 5300 Bonn 1, Mannheim, West Germany.

Hallquist, J. O., and Benson, D. J. 1987 (Jul). "DYNA3D User's Manual (Nonlinear Dynamic Analysis of Structures in Three Dimensions)," Report UCID-19592, Lawrence Livermore National Laboratory, University of California, Berkeley, CA.

Hayes, P. G. 1989 (Sep). "Backfill Effects on Response of Buried Reinforced Concrete Slabs," Technical Report SL-89-18, U.S. Army Engineer Waterways Experiment Station, Vicksburg, MS.

Hughes, T. J. R. 1987. The Finite-Element Method: Linear Static and Dynamic Finite-Element Analysis, Prentice-Hall, Inc., Englewood Cliffs, NJ.

Lysmer, J., and Kuhlemeyer, R. L. 1969 (Aug). "Finite Dynamic Model for Infinite Media," ASCE Journal of the Engineering Mechanics Division, Vol 95, No. EM4, pp. 859-877.

Pelessone, D. 1989 (Jan). "A Modified Formulation of the Cap Model," Draft Report GA-C19579, General Atomics, San Diego, CA, prepared for the Defense Nuclear Agency, Washington, DC.

Sandler, I. S., and Rubin, D. 1979. "An Algorithm and a Modular Subroutine for the Cap Model," International Journal of Numerical Analysis Methods in Geomechanics, 3, pp 173-186.

Simo, J. C., Ju, J. W., Pister, K. S., and Taylor, R. L. 1985 (May). "An Assessment of the Cap Model: Consistent Return Algorithms and Rate Dependent Extension," Report No. UCB/SESM-85/5, Department of Civil Engineering, University of California, Berkeley, CA.

Underwood, P. G., and Geers, T. L. 1978 (Mar). "Doubly Asymptotic, Boundary-Element Analysis of Dynamic Soil-Structure Interaction," DNA Report 4512T, Defense Nuclear Agency, Washington, DC.

Underwood, P. G., and Geers, T. L. 1979 (Jun). "Doubly Asymptotic, Boundary-Element Analysis of Non-Linear Soil-Structure Interaction," DNA Report 4953F, Defense Nuclear Agency, Washington, DC.

U.S. Army Engineer Waterways Experiment Station. 1986 (Nov). "Fundamentals of Protective Design for Conventional Weapons," Army Technical Manual 5-855-1, Vicksburg, MS.

Weidlinger, P., and Hinman, E. 1978 (Jul). "Analysis of Underground Protective Structures," ASCE Journal of Structural Engineering, Vol 114, No. 7, pp. 1658-1673.

Zimmerman, H. D., and others. 1990 (Jun). "Ground Shock Environment from Subscale Munition Tests; CONWEB 1 and 2 Events, 15.4 lb C4 in Wet Clay Backfill," CRT Report 3295-02, California Research and Technology, Inc., Chattsworth, CA.

Zimmerman, H. D., and others. 1990 (Oct). "Ground Shock Environment from Subscale Munition Test; CONWEB 3 Event, 15.4 lb C4 in Dry Sand Backfill," CRT Report 3295-020-2, California Research and Technology, Inc., Chattsworth CA.

Table 1

Properties of Clay and Sand

Parameter*	Units	Clay	Sand
K_1	psi	1.16×10^6	2.219×10^6
K_1	$psi^{(1-K2)}$	312	312
K_2		0.7	0.7
G	psi	43,511	1.088×10^6
α	psi	16.68	18,564.69
θ		0.0	0.0
B	1/psi	0.00434	2.530×10^{-5}
γ	psi	13.78	18,562.51
R		2.5	3.5
D1	1/psi	0.00138	7.585×10^{-5}
D2	$1/psi^2$	0.00	0.00
W		0.04	0.256
X_0	psi	0.00	0.00
ρ	$lb\text{-}sec^2/in.^4$	1.841×10^{-4}	1.752×10^{-4}
T	psi	0.00	0.00

Table 2

Parameters for Grid Spacing Runs

Run	e_{Max}	% tcrit	Viscosity Factor
6-degree constant aspect ratio	0.00001	10	10
2-degree constant aspect ratio	0.00001	10	10
1-in. constant radial spacing	0.0001	10	5

* Parameters are defined in paragraphs 24-26.

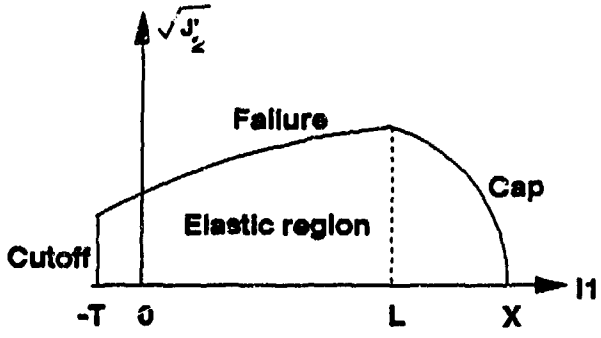

Figure 1. Failure surface for cap model in DYNA3D

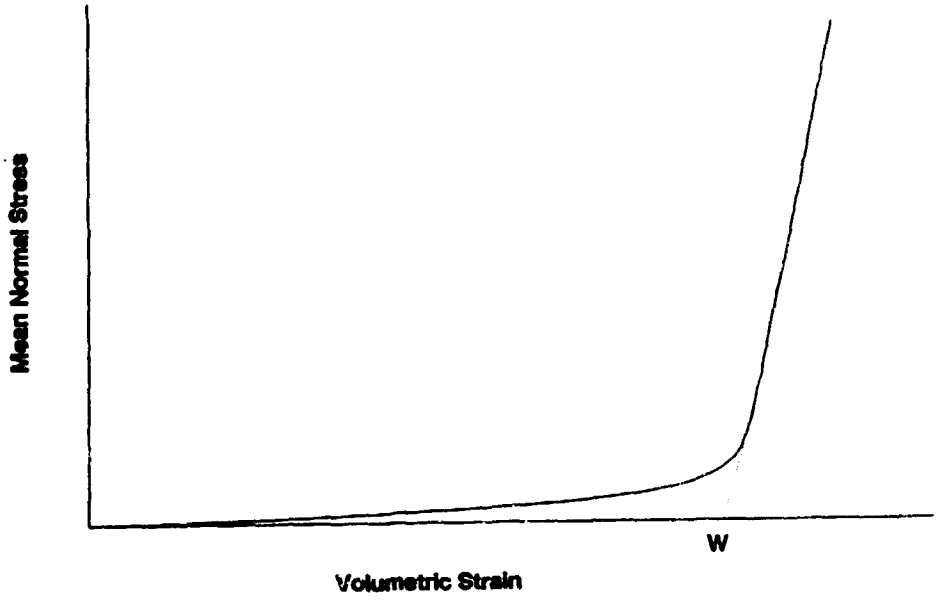

Figure 2. Hardening function in DYNA3D cap model

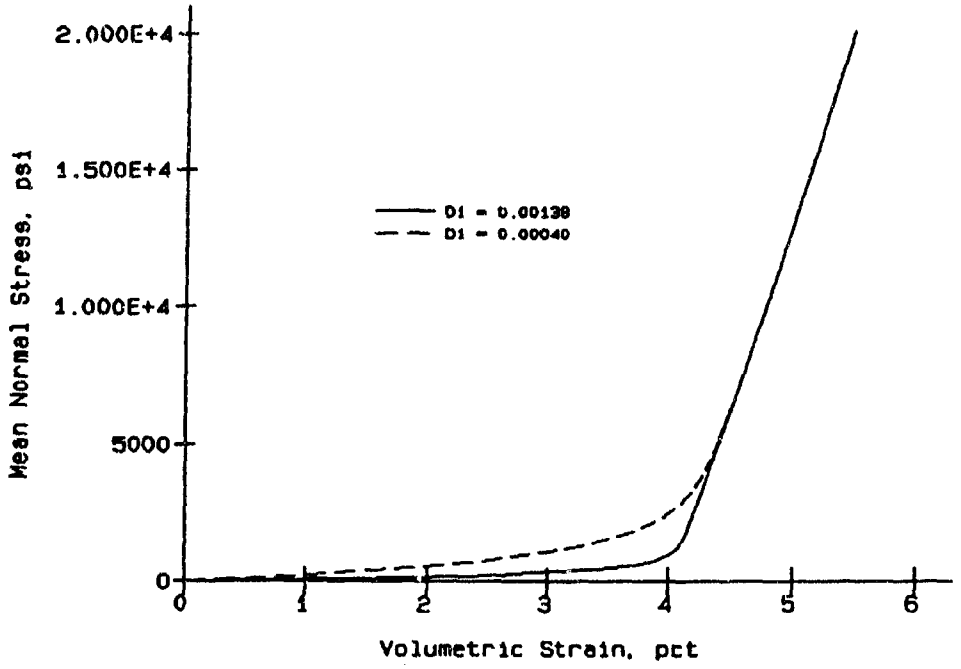

Figure 3. Comparison of hydrostatic stress-strain curves for clay

Figure 4. One-dimensional spherical grid

Element 1 Nodes 1, 2, 3, and 4
Element 2 Nodes 5, 3, 2, and 4

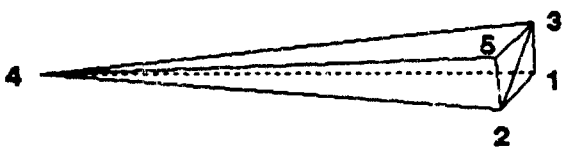

Figure 5. Four-node element for charge

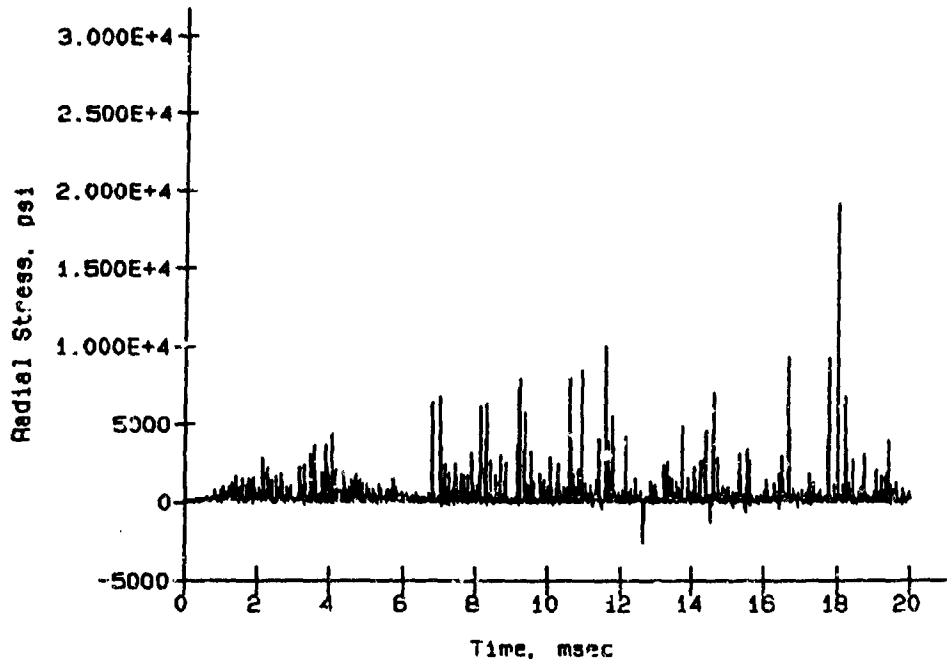

Figure 6. Stress time-history for unstable run

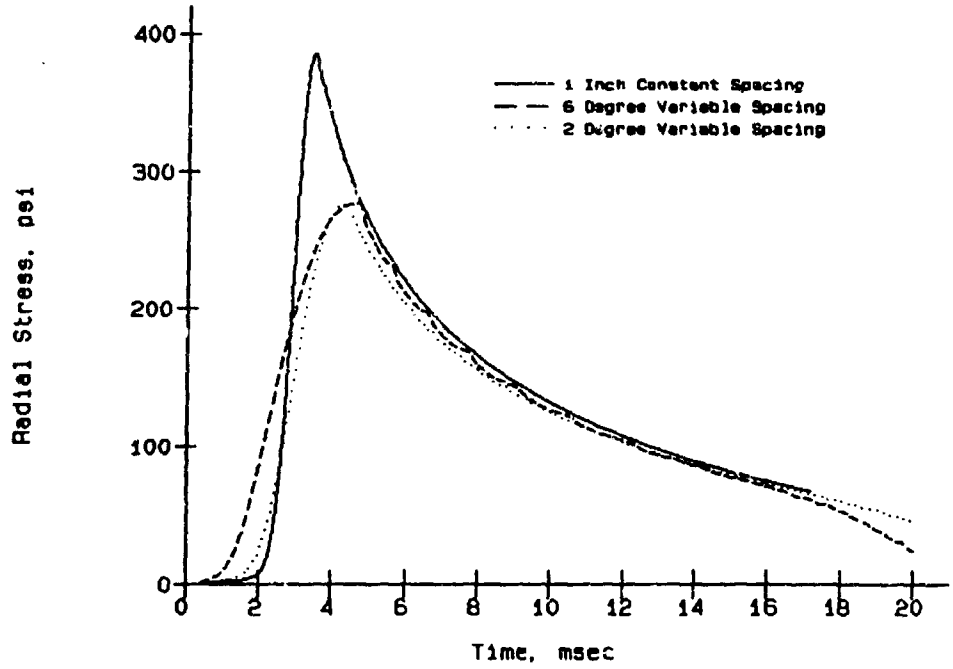

Figure 7. Comparison of grids with constant and variable radial spacing

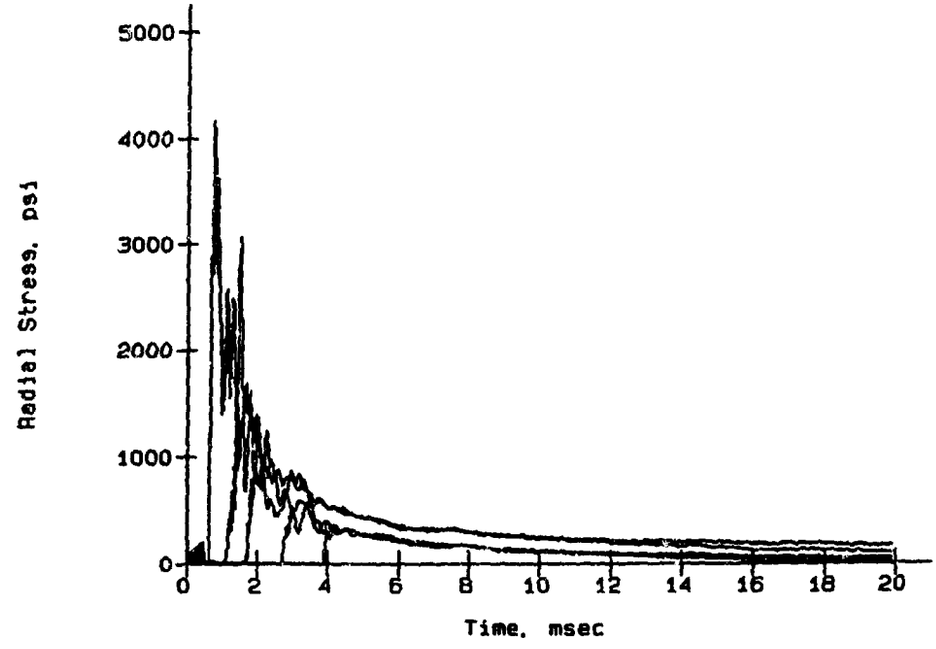

a. Measured

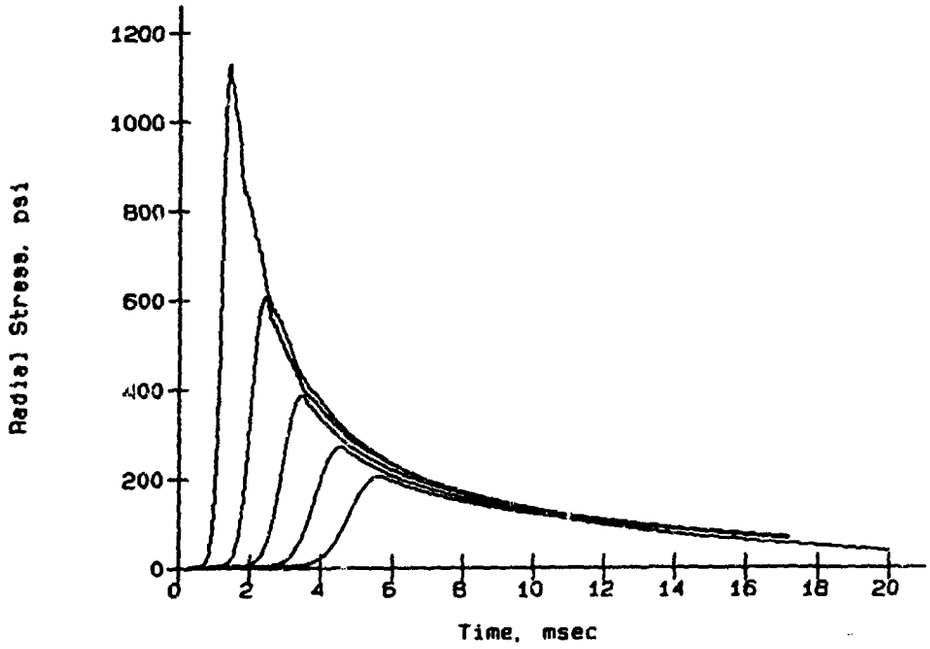

b. Computed

Figure 8. Comparison of computed (4-in. sphere) to measured radial stresses

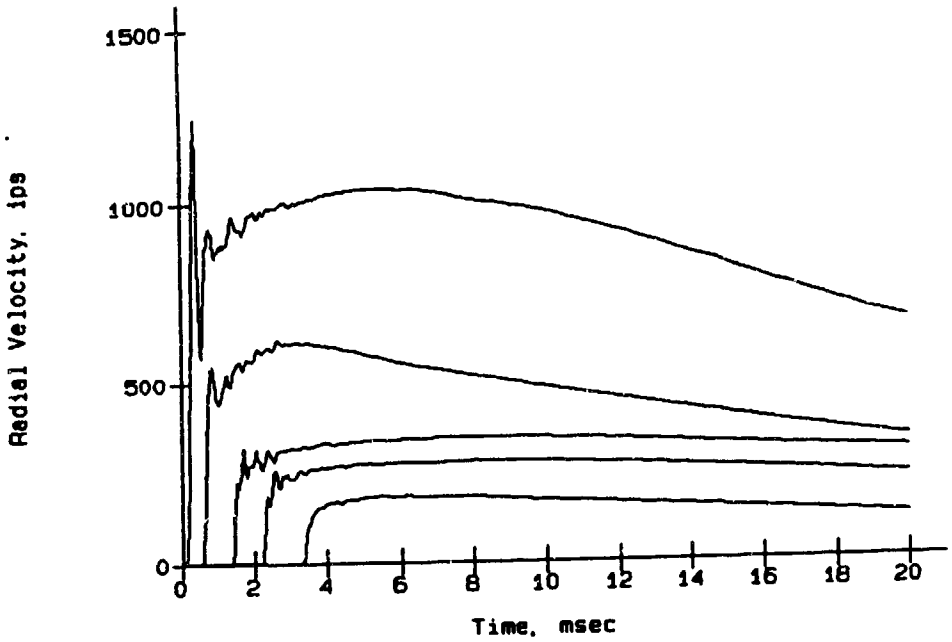

a. Measured

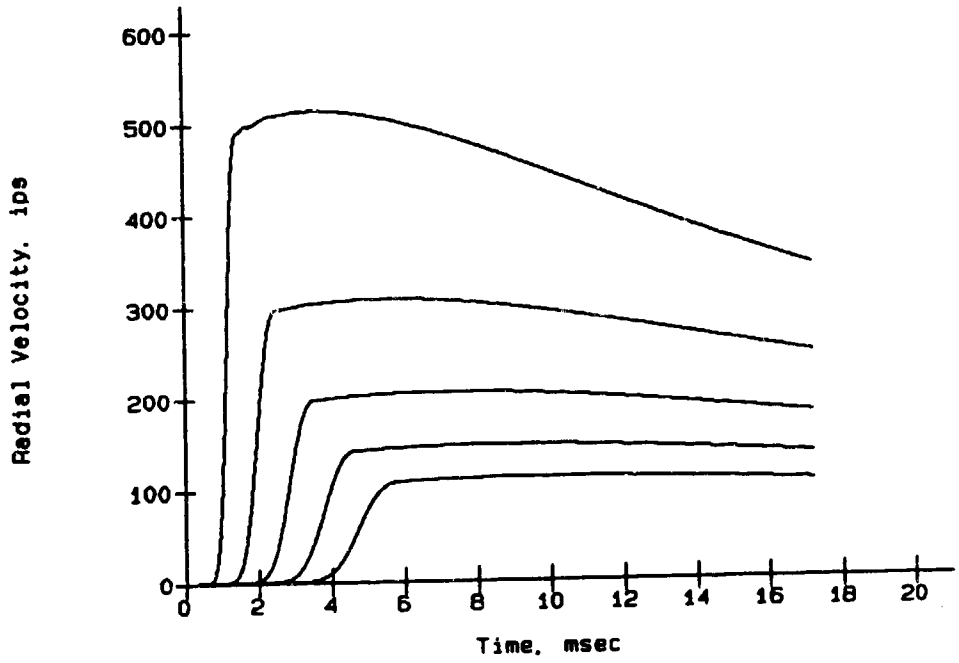

b. Computed

Figure 9. Comparison of computed (4-in. radius) to measured radial velocities

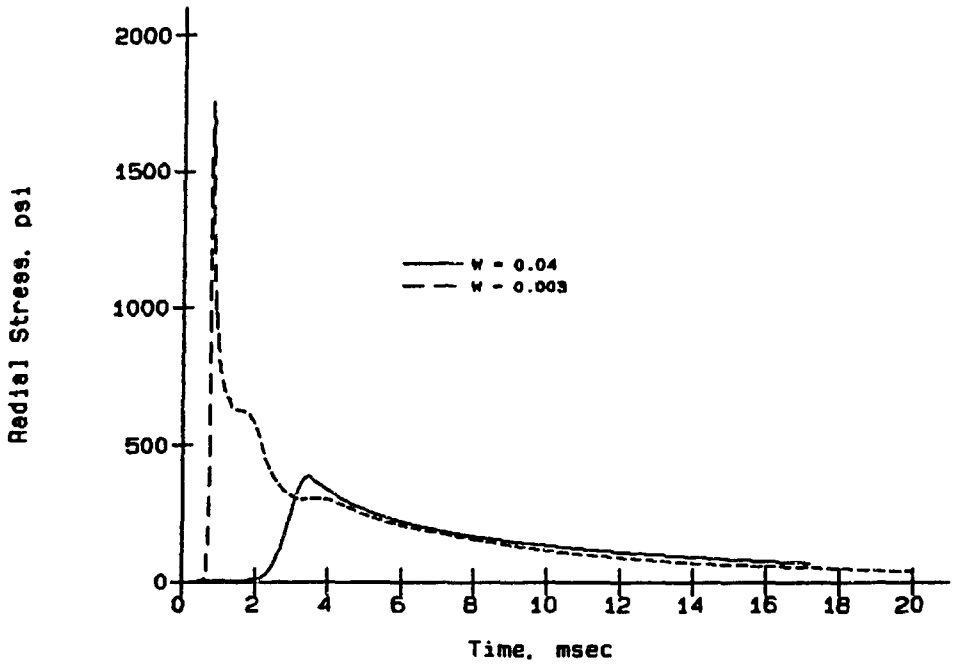

Figure 10. Effect of changes in material properties on stress time-history

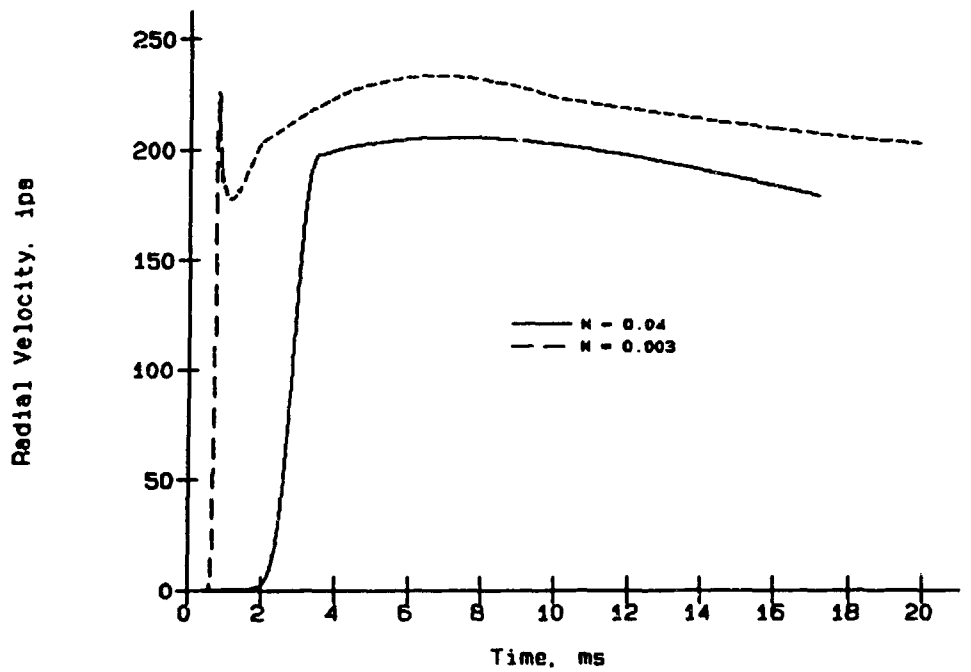

Figure 11. Effect of changes in material properties on velocity time-history

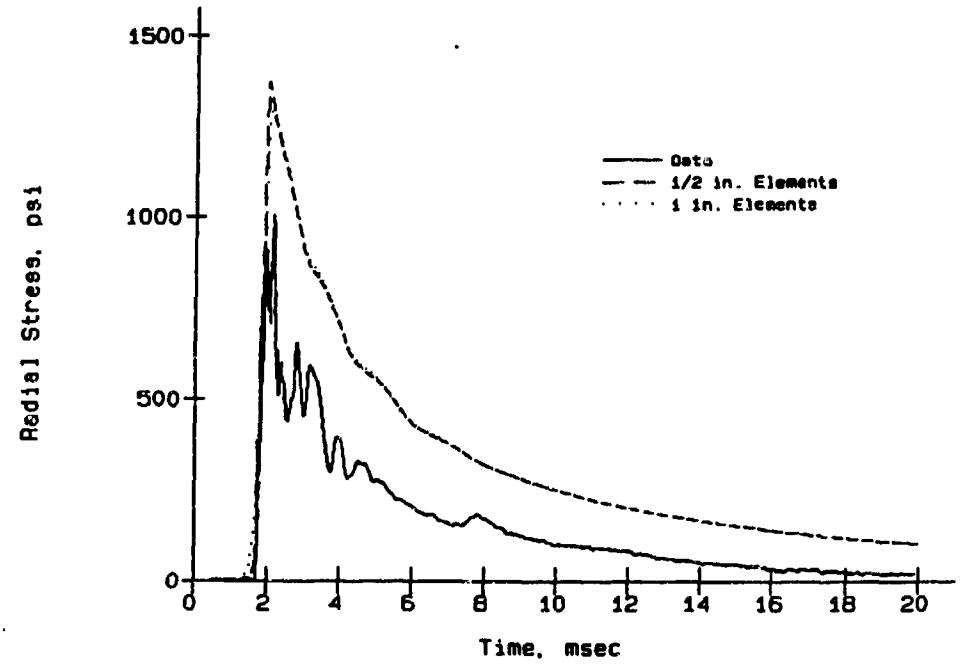

Figure 12. Effect of grid spacing on stress time-history

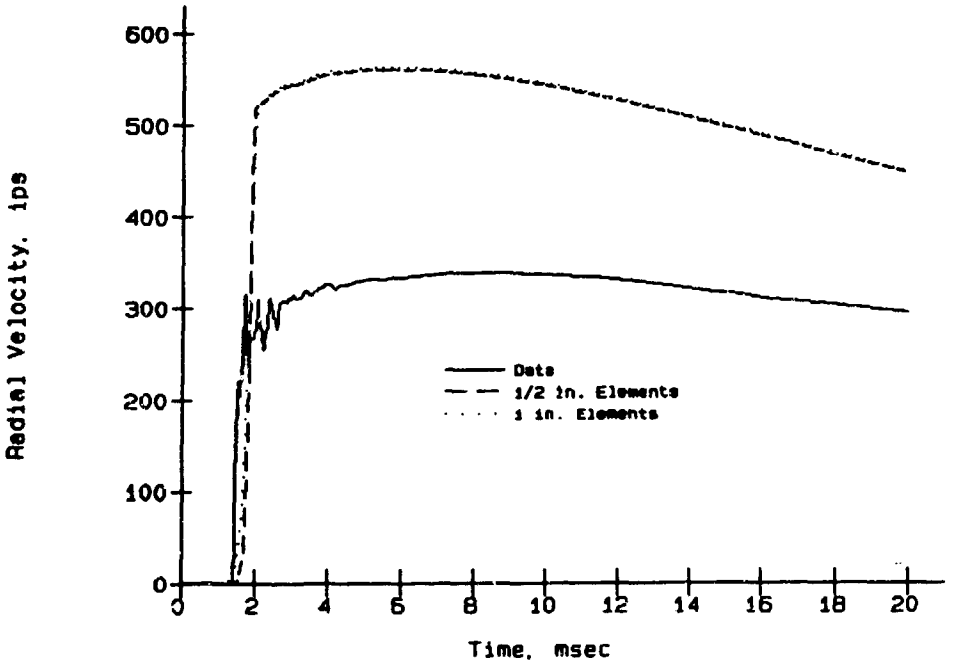

Figure 13. Effect of grid spacing on velocity time-history

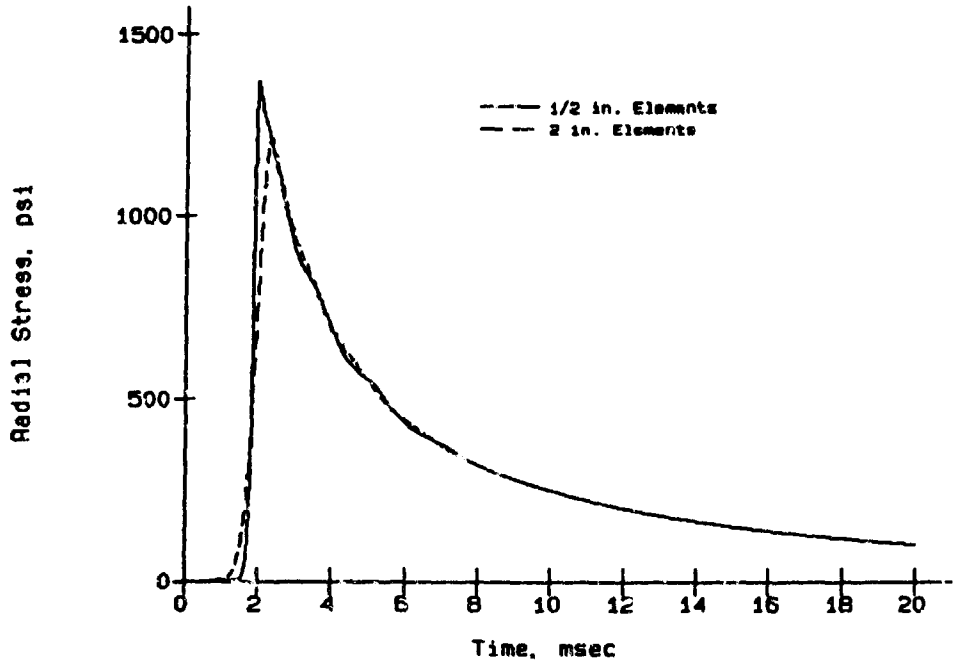

Figure 14. Effect of 1/2-in. vs 2-in grid spacing on stress time-history

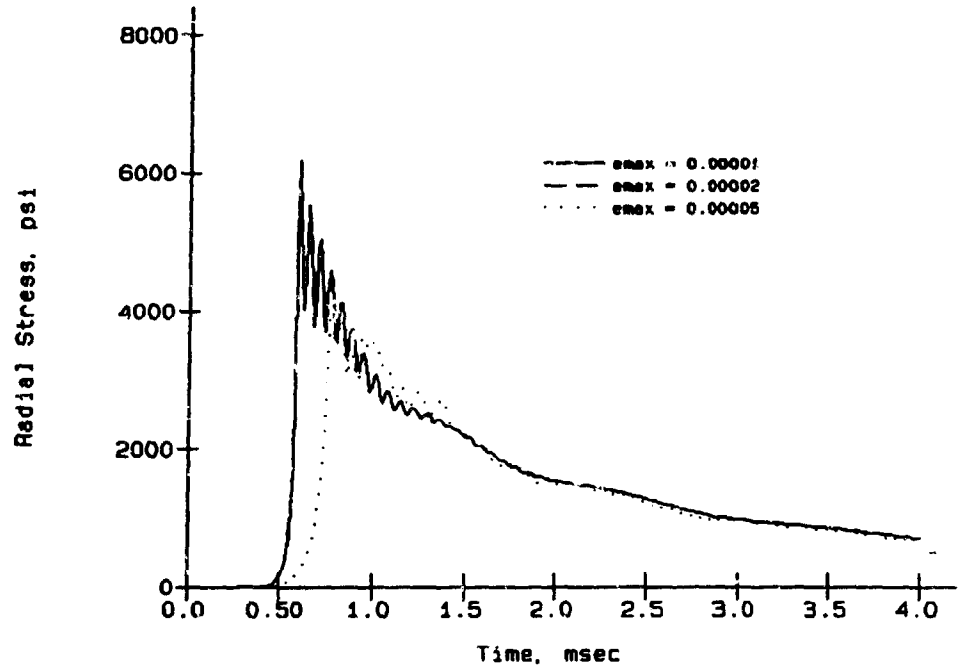

Figure 15. Effect of changes in maximum strain increment on stresses at 3 ft

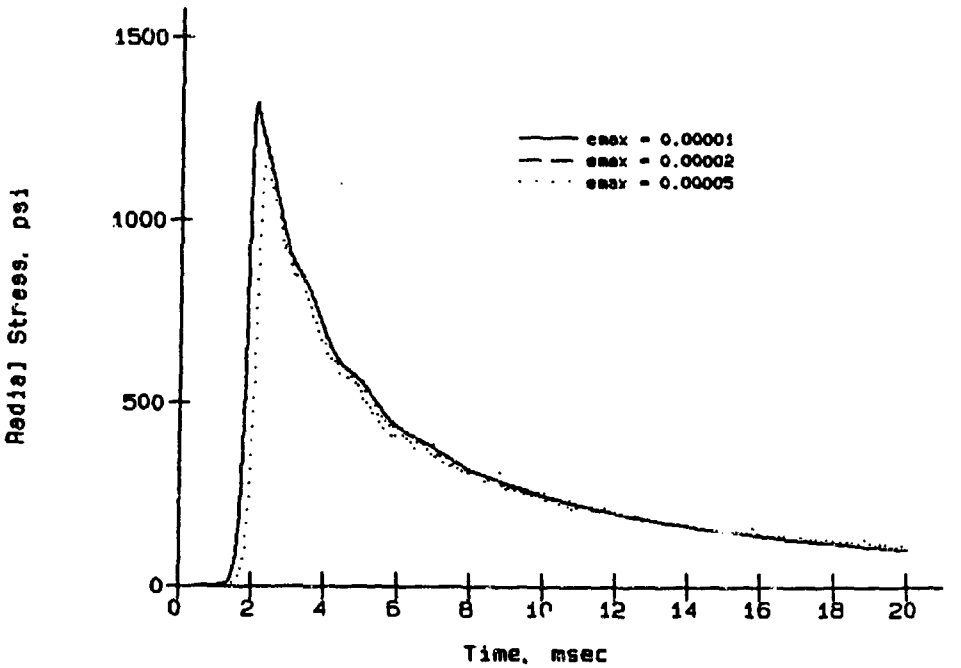

Figure 16. Effect of changes in maximum strain increment on stresses at 5 ft

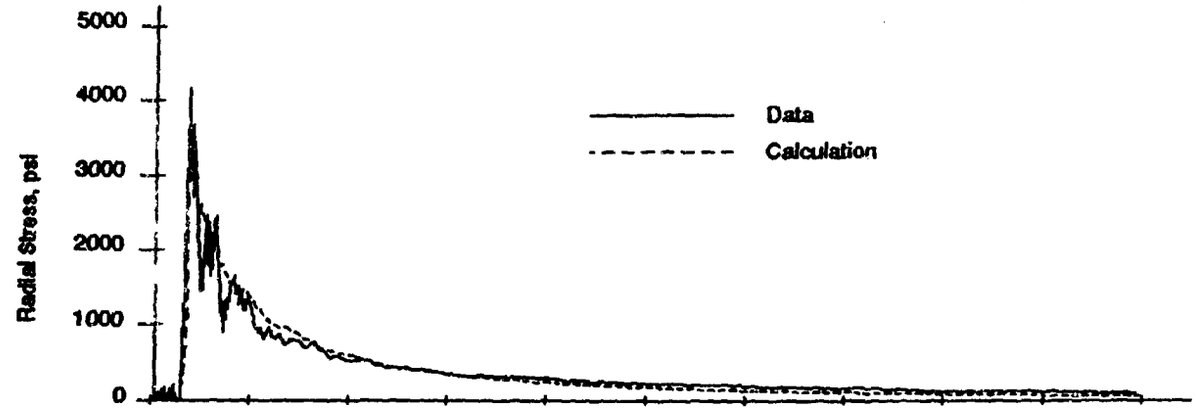

a. Range = 3 ft

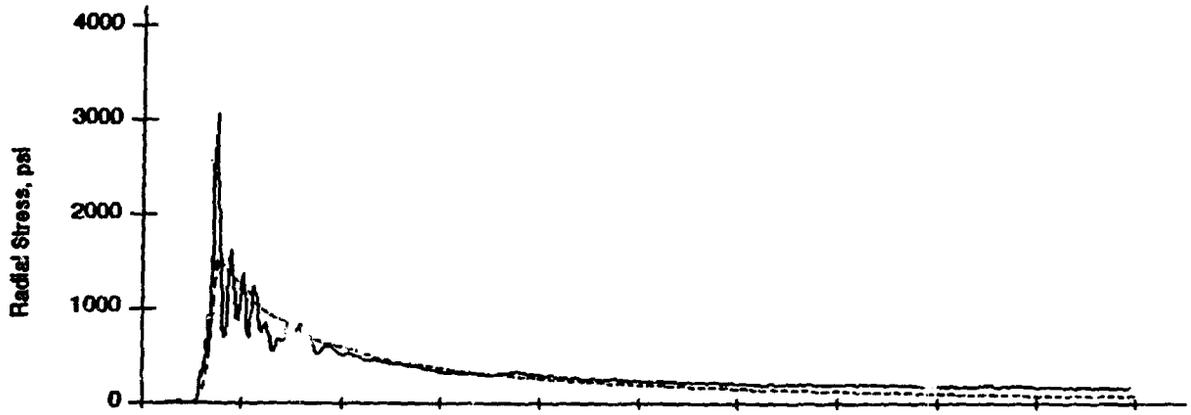

b. Range = 4 ft

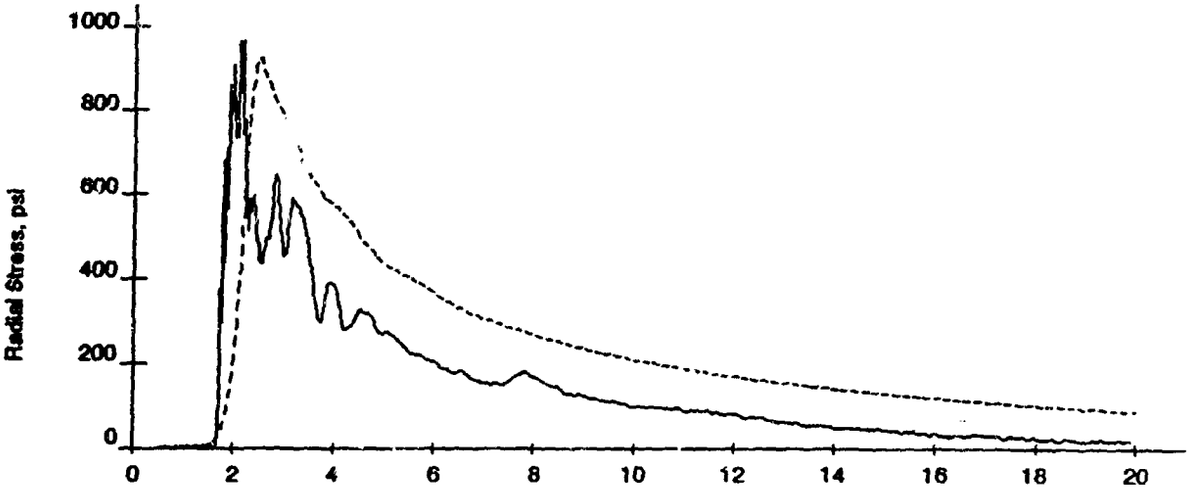

c. Range = 5 ft

Figure 17. Comparison of measured to computed radial stresses (continued)

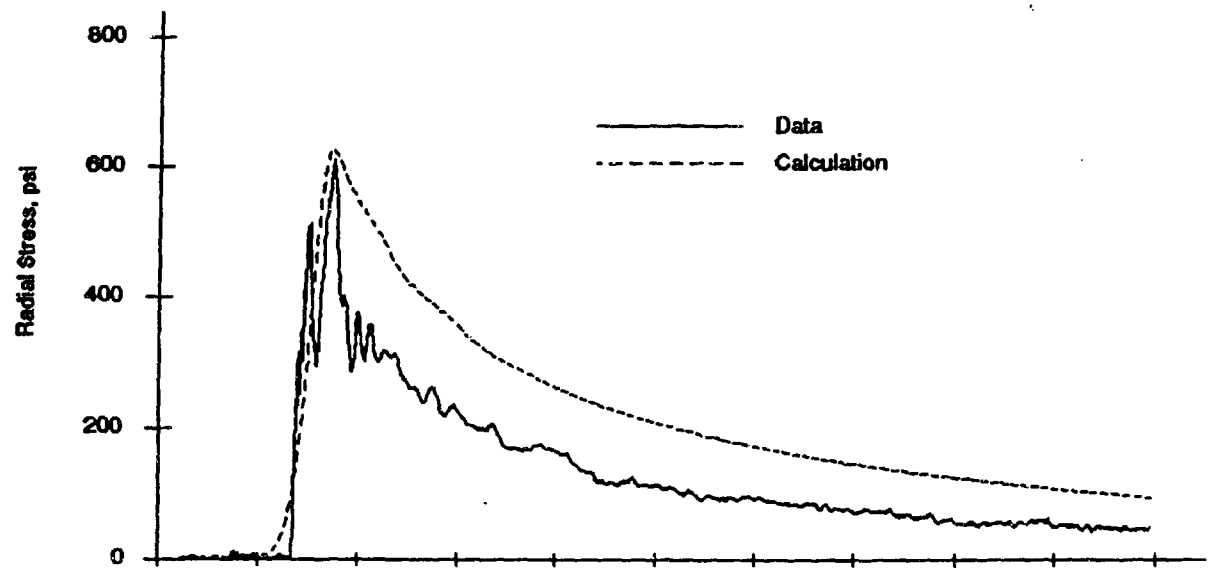

d. Range = 6 ft

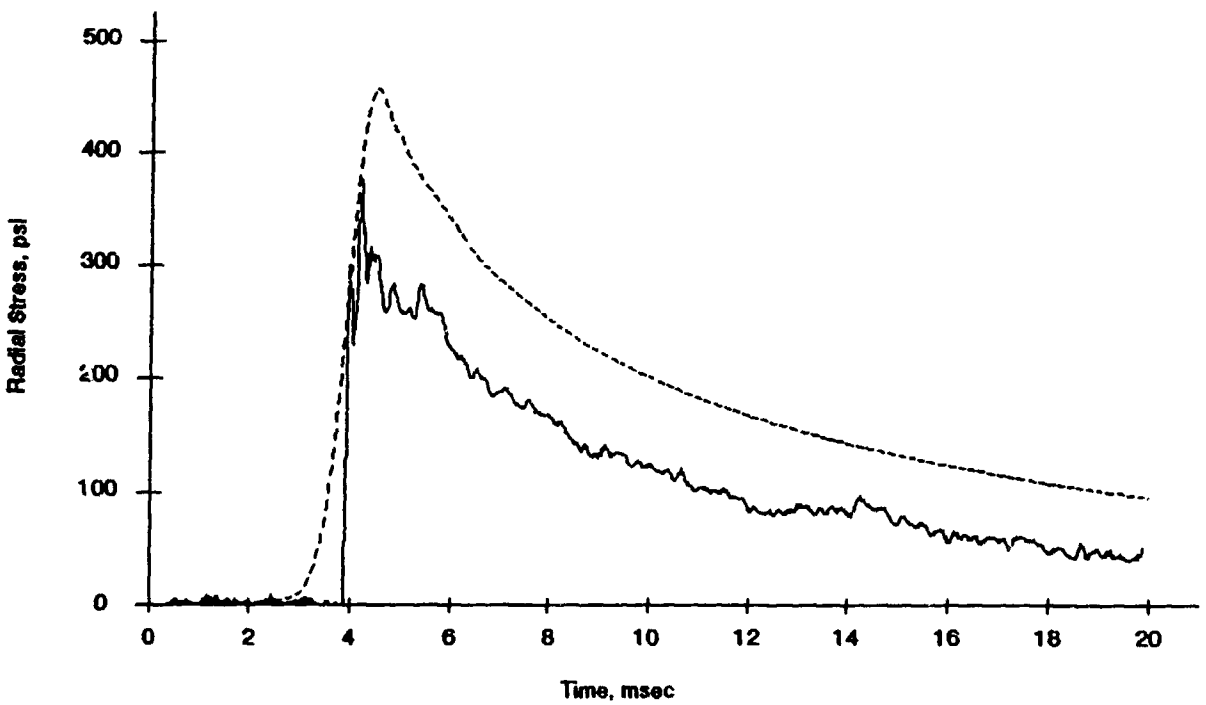

e. Range = 7 ft

Figure 17. (Concluded)

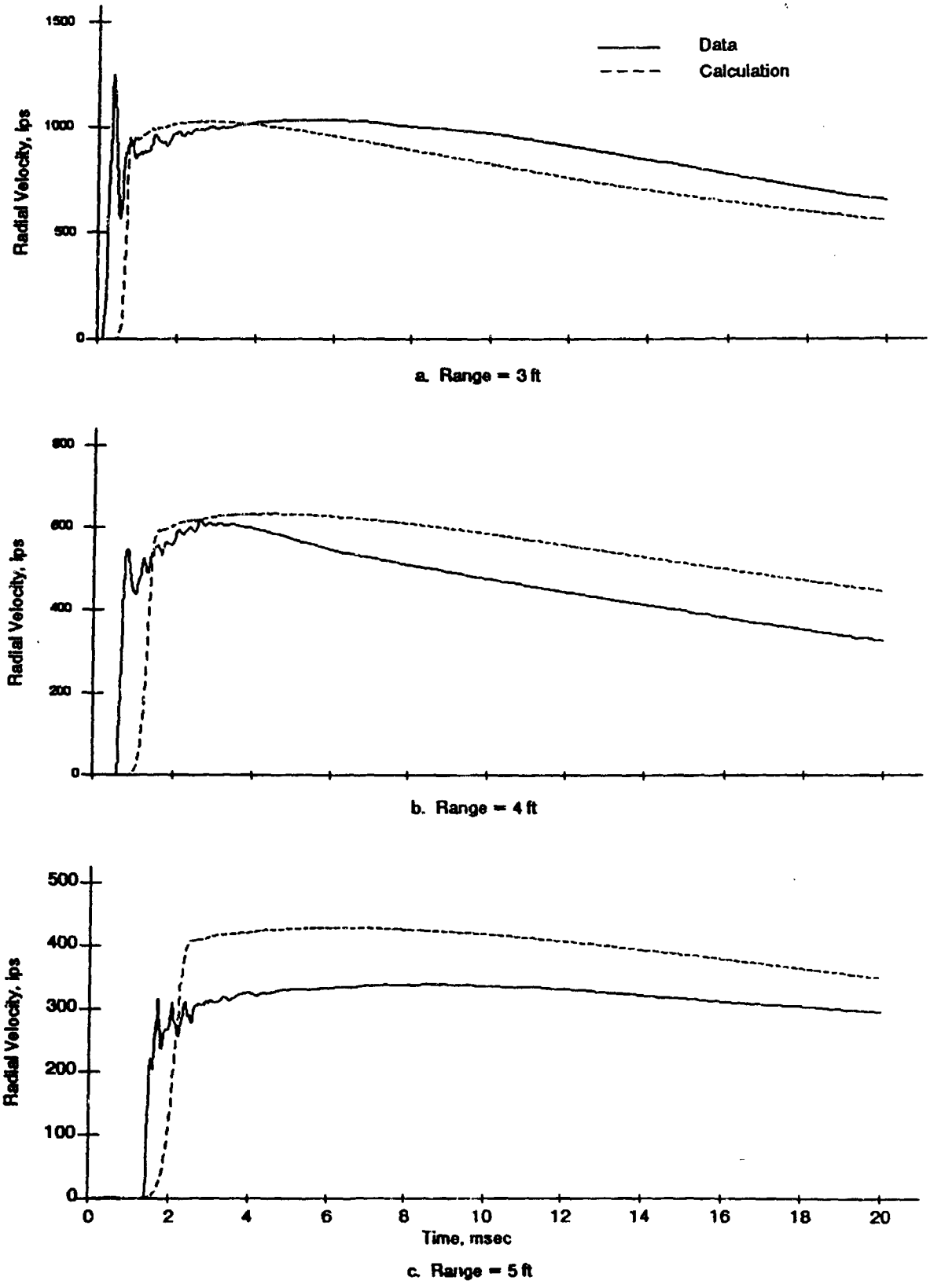

Figure 18. Comparison of measured to computed radial velocities (continued)

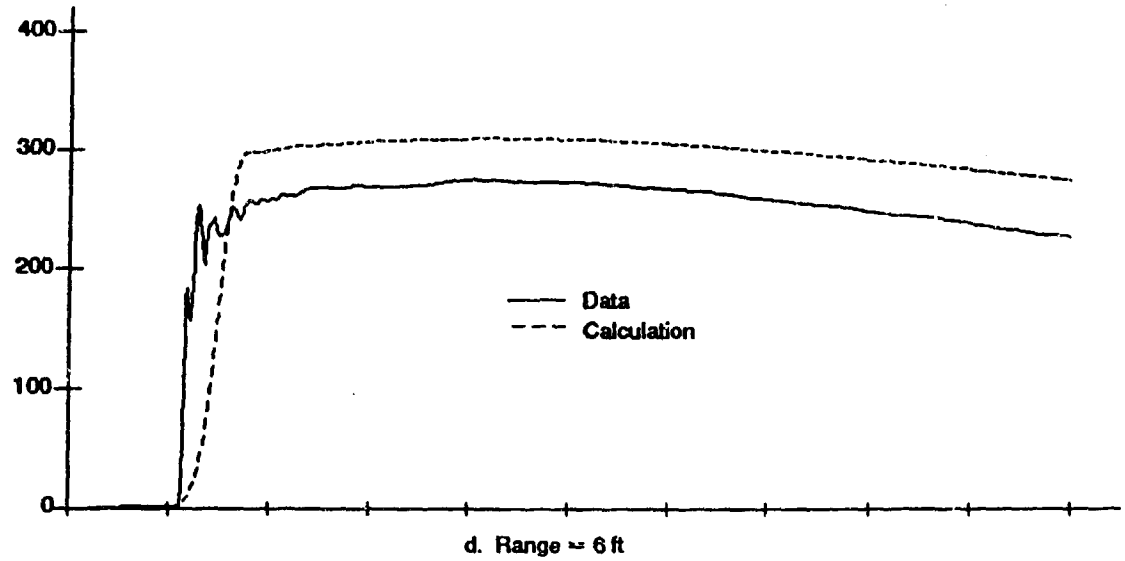

d. Range ≈ 6 ft

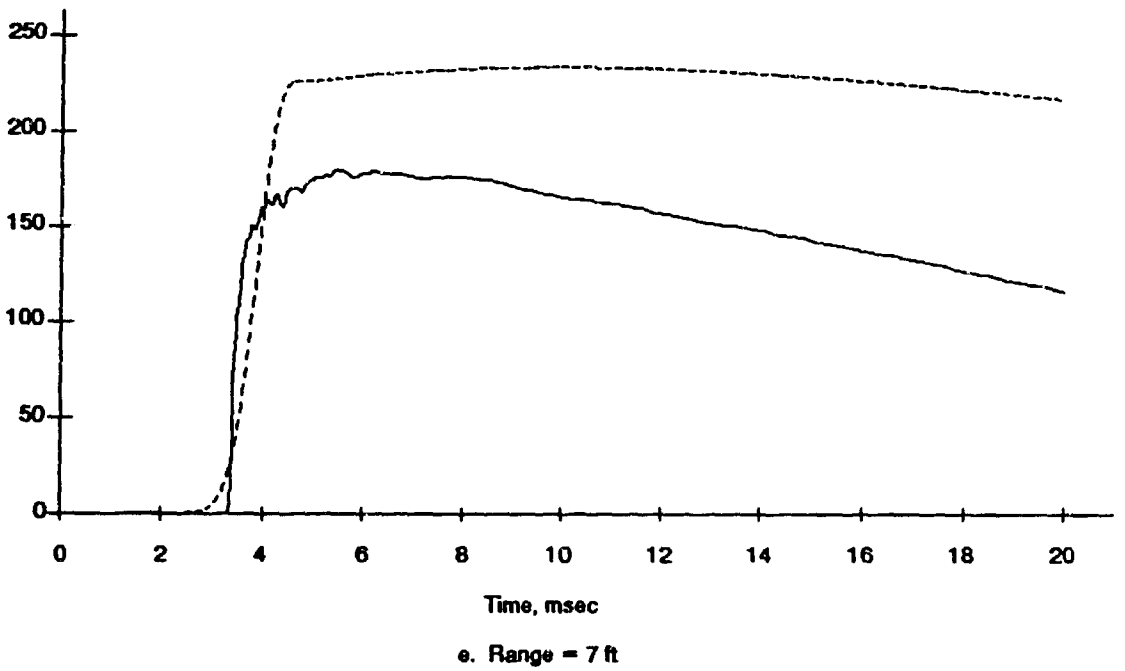

e. Range = 7 ft

Figure 18. (Concluded)

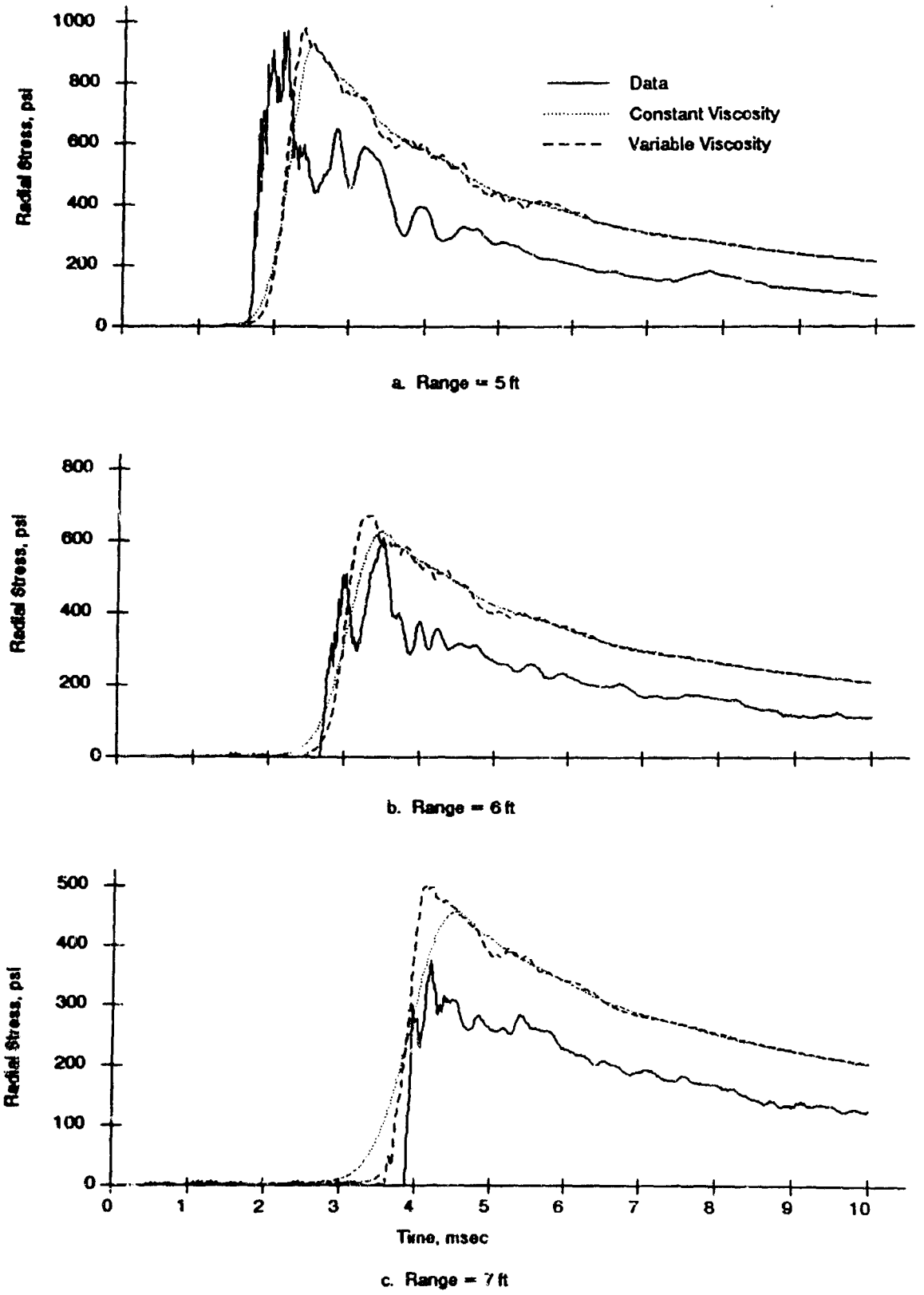

Figure 19. Effect of variable artificial viscosity on stresses

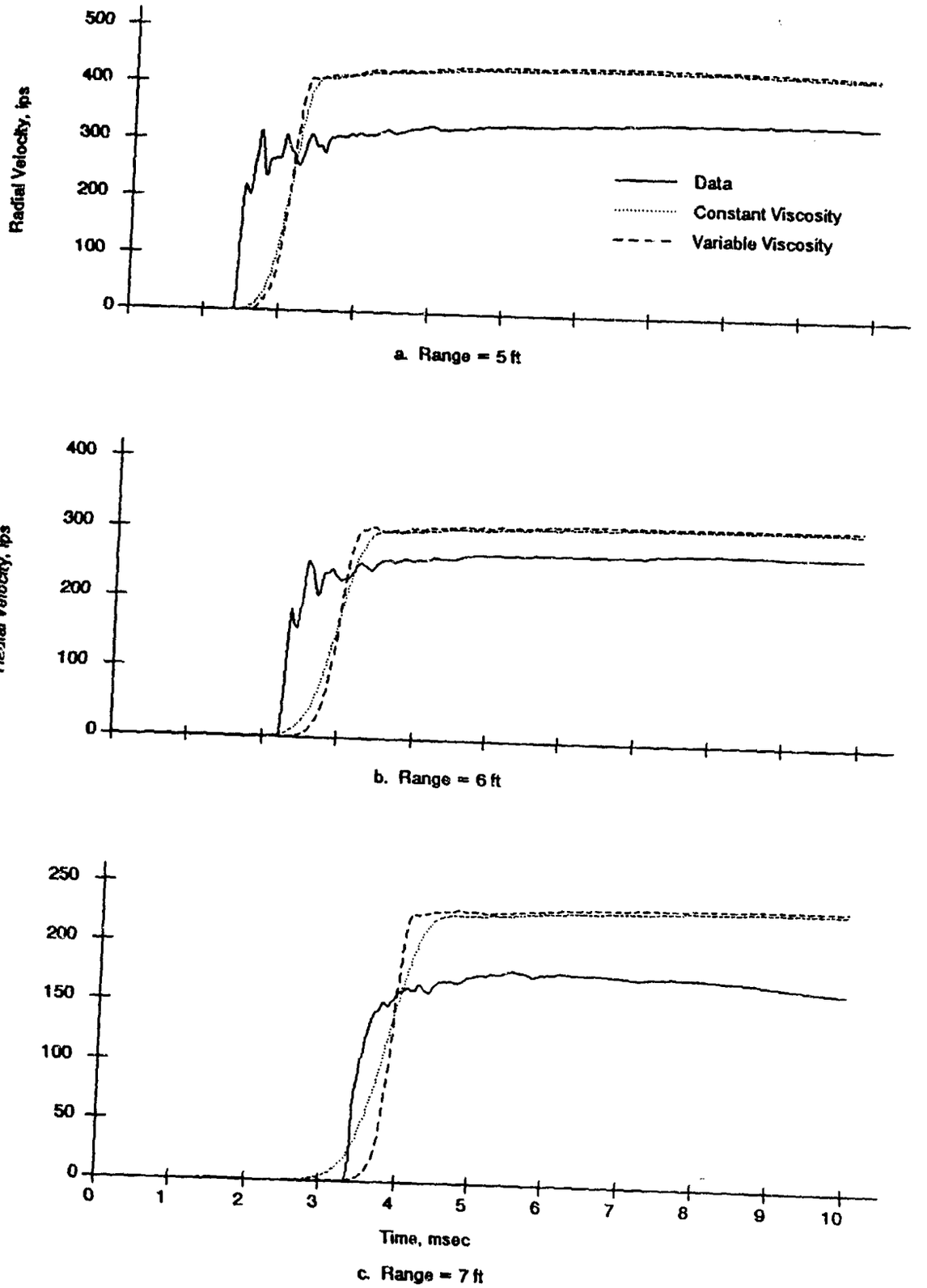

Figure 20. Effect of variable artificial viscosity on velocity

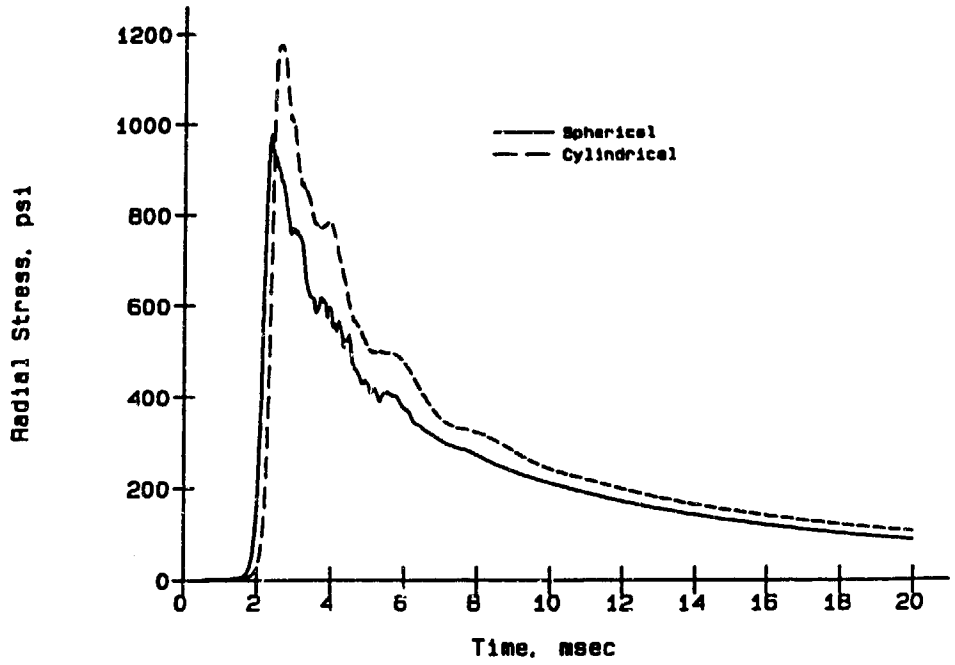

Figure 21. Comparison of cylindrical to spherical geometry (stresses at 5 ft)

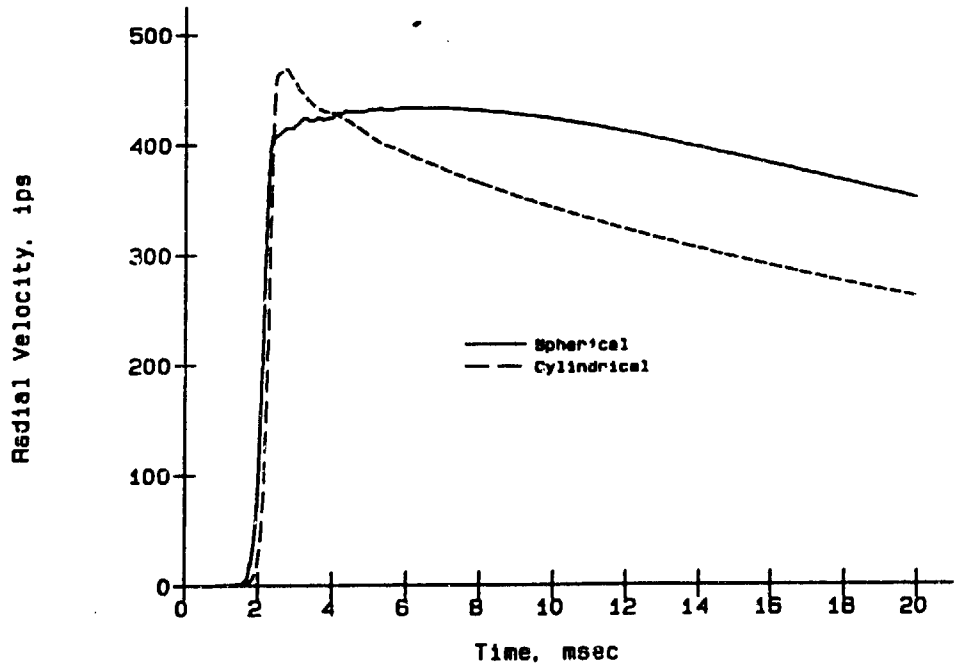

Figure 22. Comparison of cylindrical to spherical geometry (velocities at 5 ft)

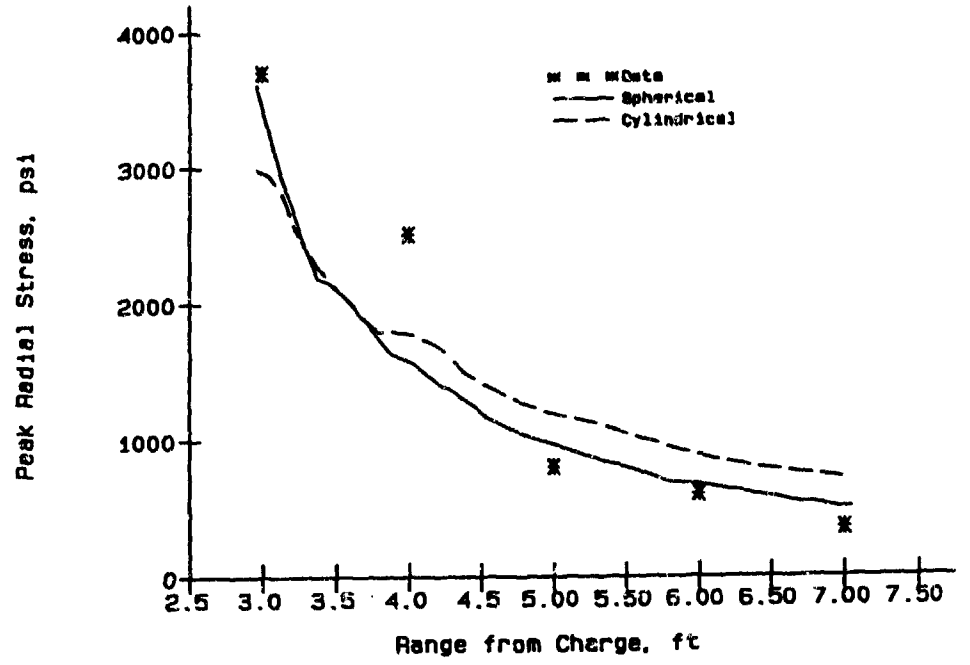

Figure 23. Comparison of cylindrical to spherical (peak stress versus range)

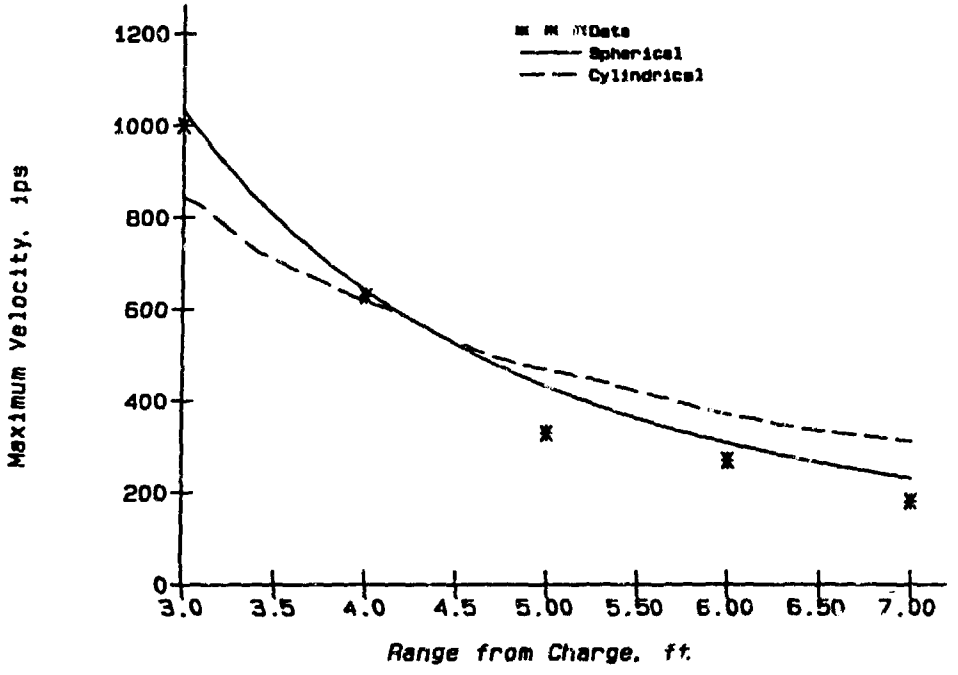

Figure 24. Comparison of cylindrical to spherical (peak velocity versus range)

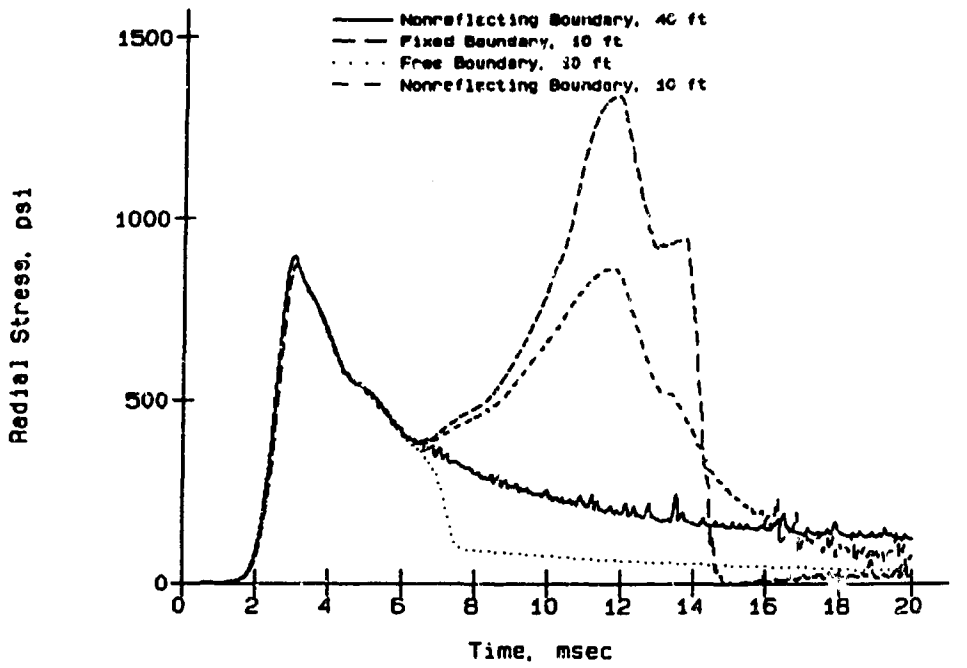

Figure 25. Effect of boundary conditions, stresses at 5 ft

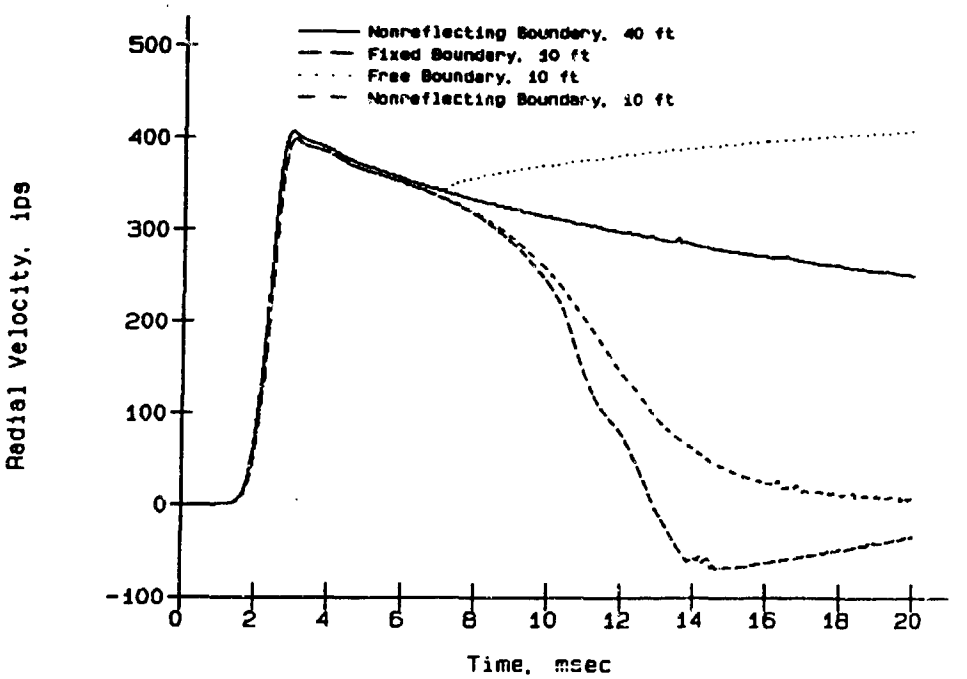

Figure 26. Effect of boundary conditions, velocities at 5 ft

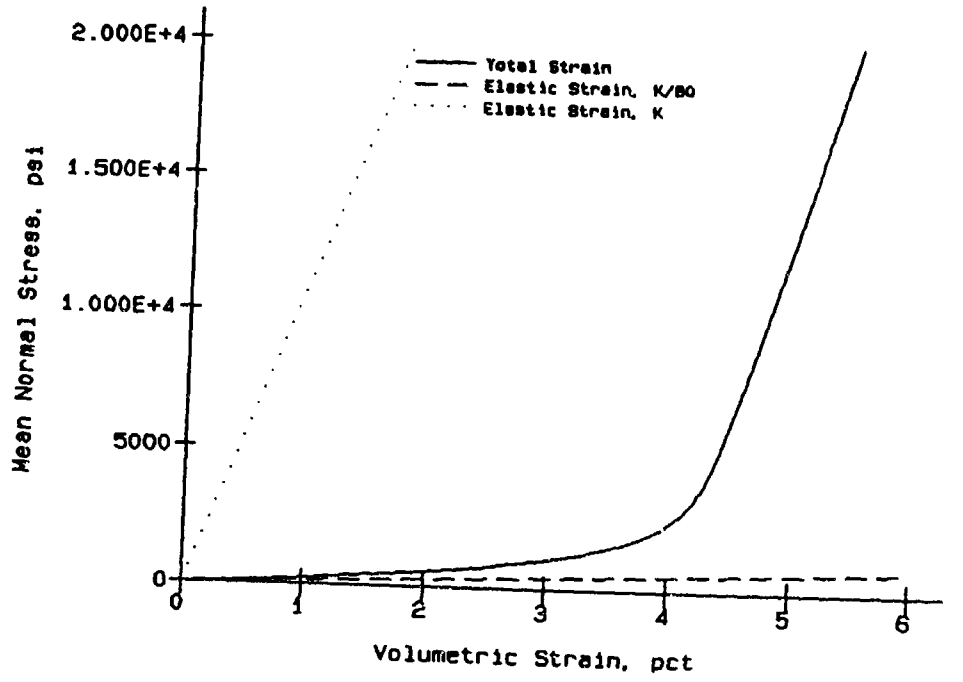

Figure 27. Comparison of elastic to total hydrostatic stress-strain curves

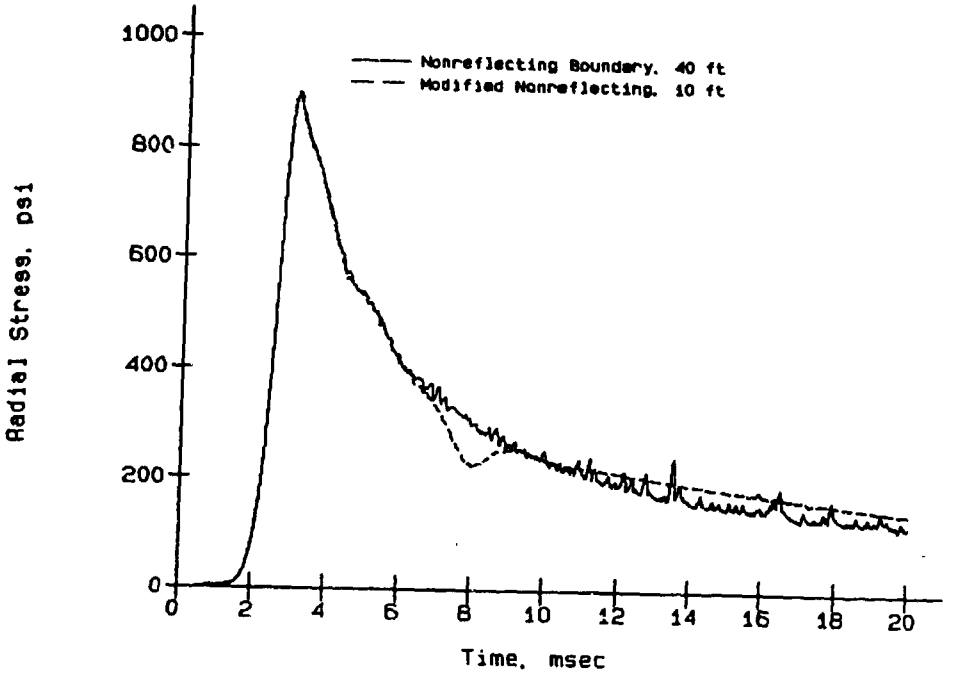

Figure 28. Effect of modified nonreflecting boundary on stresses at 5 ft

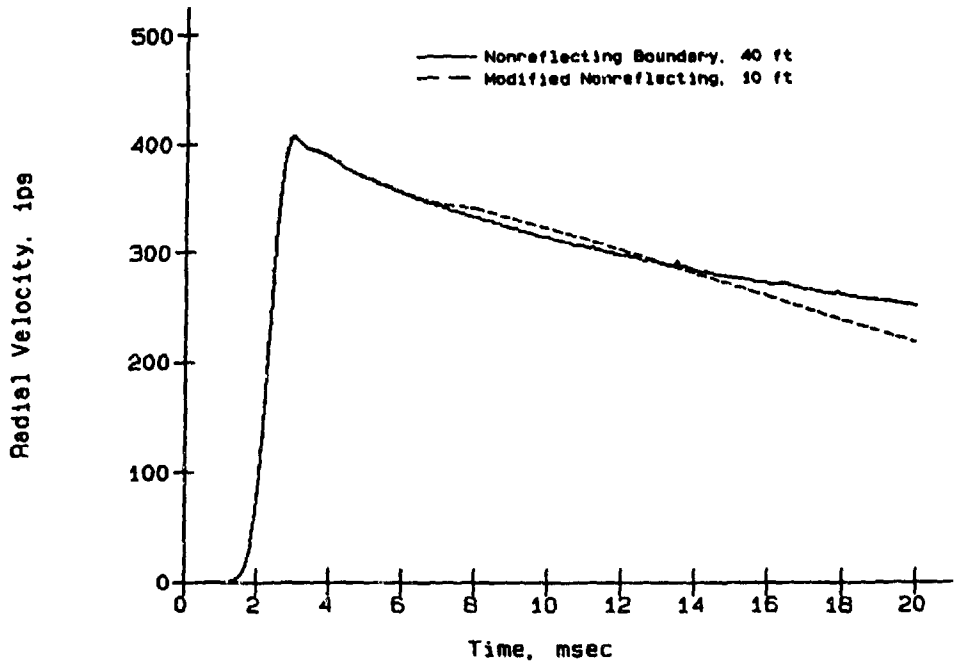

Figure 29. Effect of modified nonreflecting boundary on velocities at 5ft

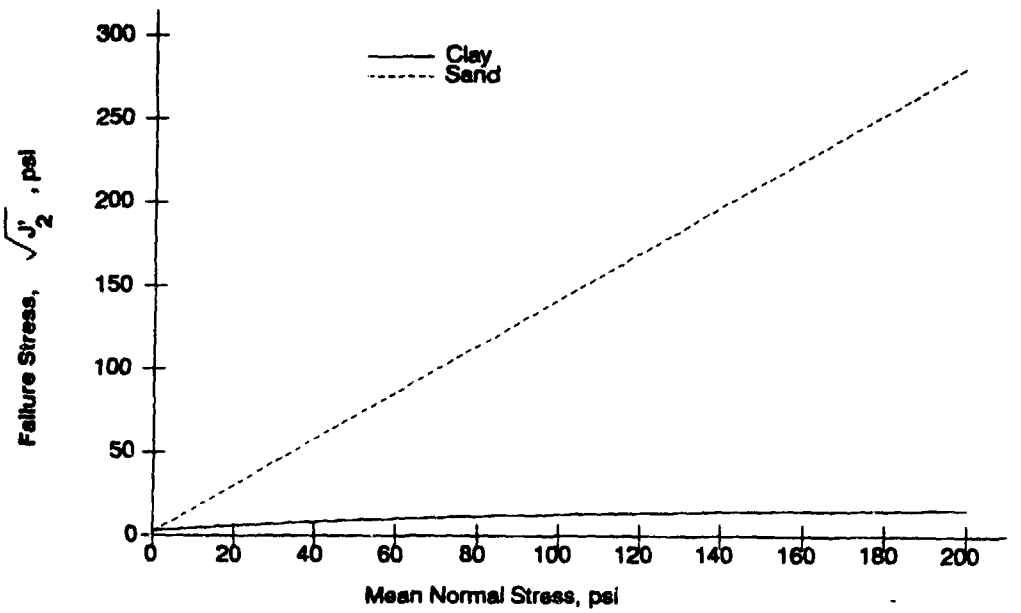

Figure 30. Comparison of clay and sand failure surfaces

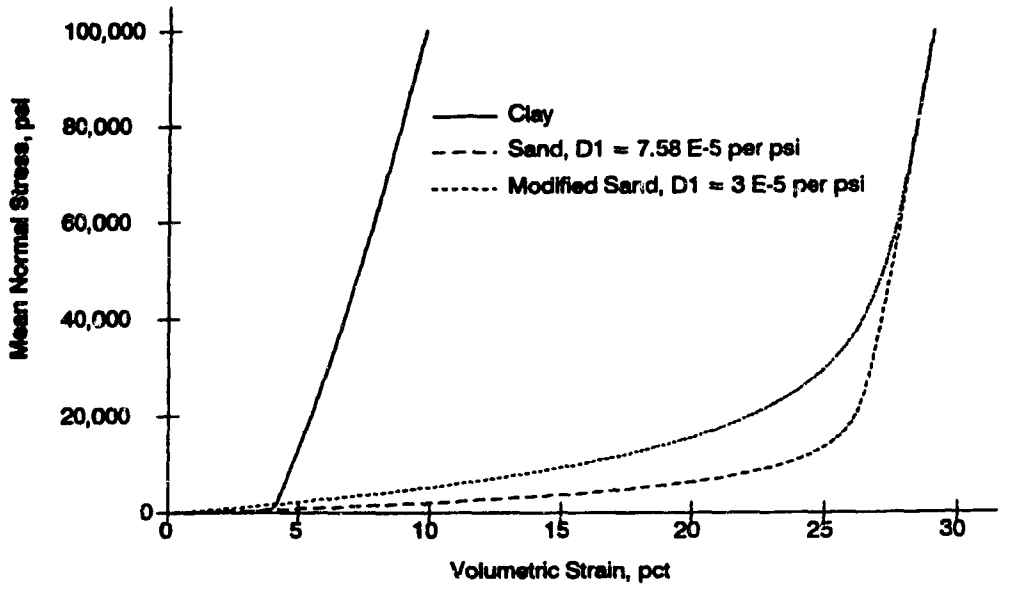

Figure 31. Comparison of Hydrostatic stress-strain curves for clay and sand

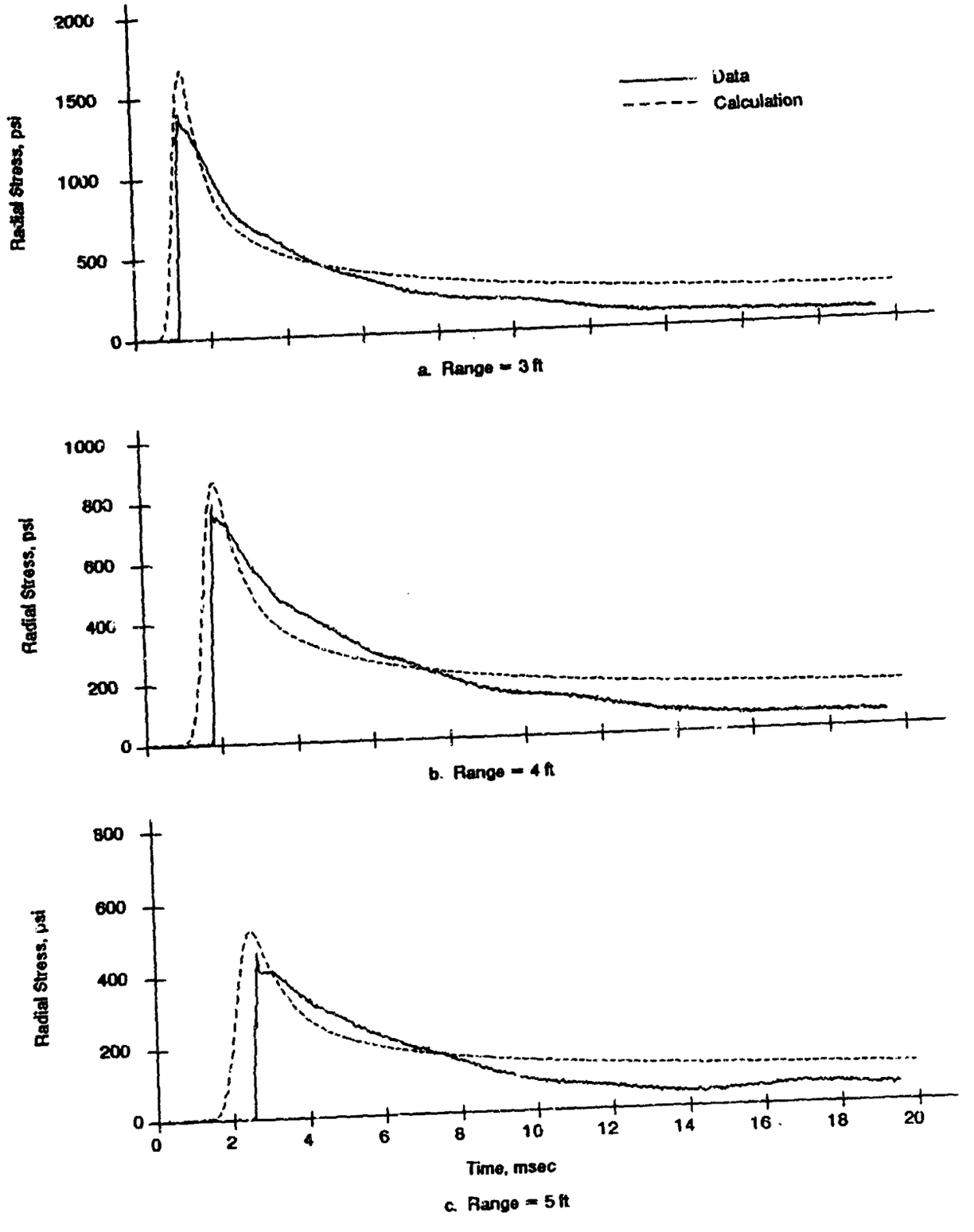

Figure 32. Comparison of measured to computed radial stresses for sand (continued)

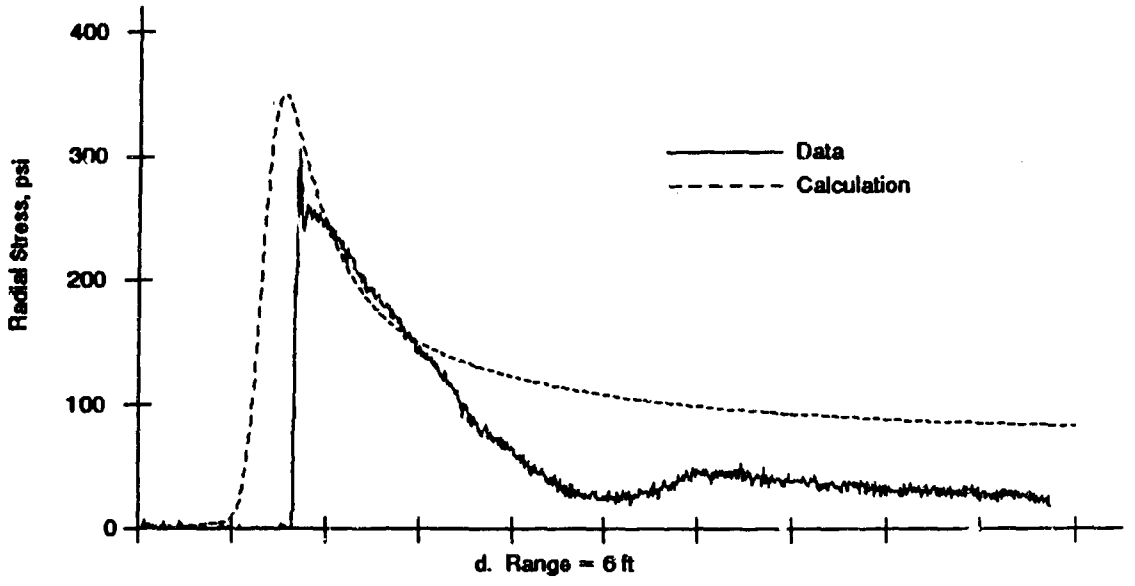

d. Range = 6 ft

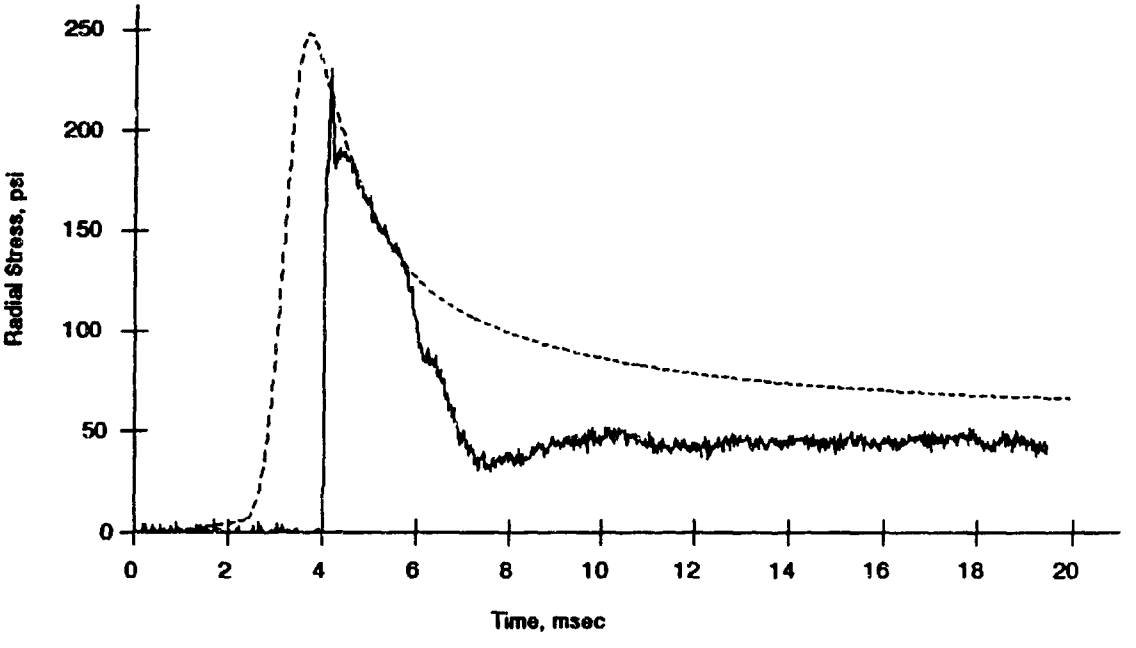

e. Range = 7 ft

Figure 32. (Concluded)

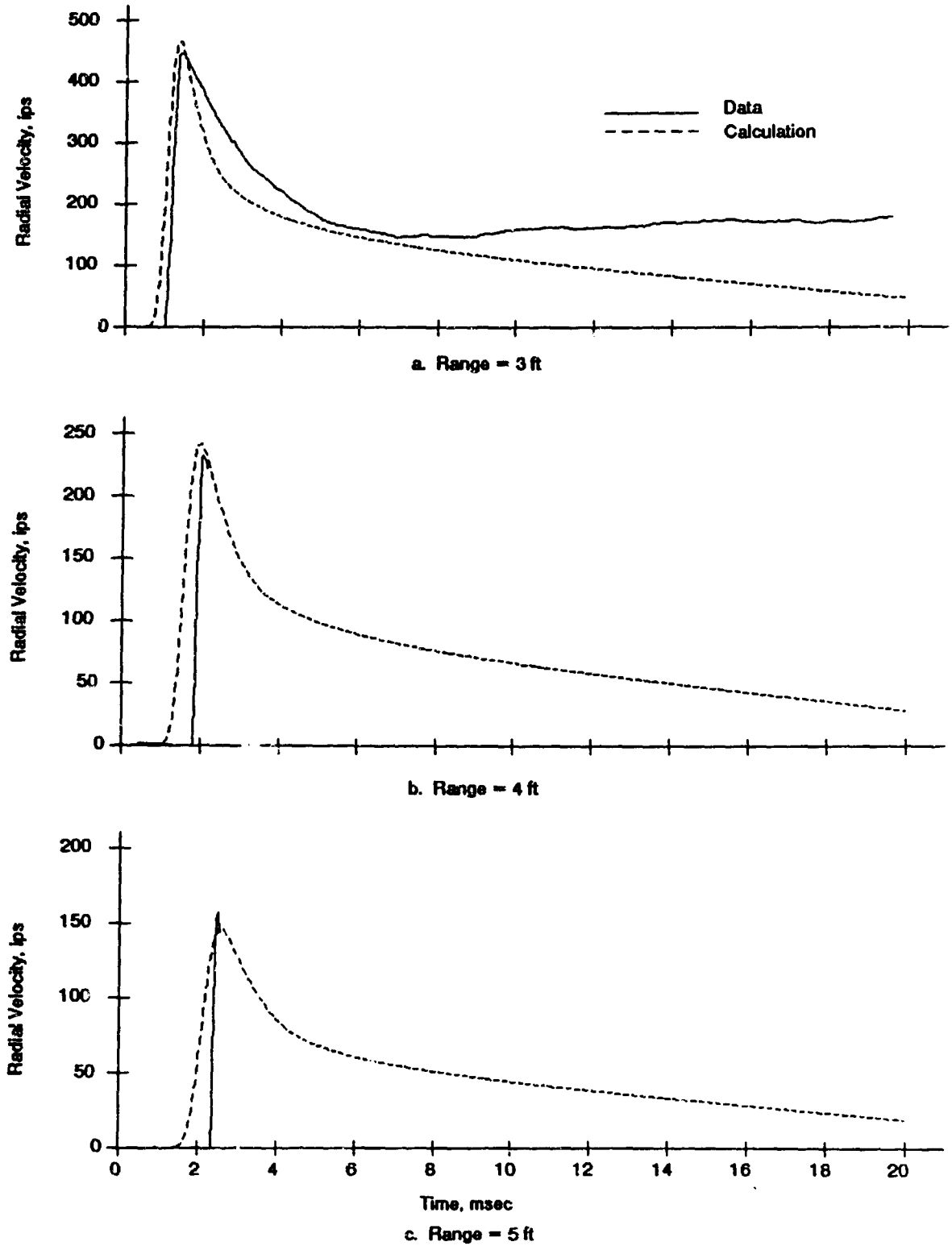

Figure 33. Comparison of measured to computed radial velocities for sand (continued).

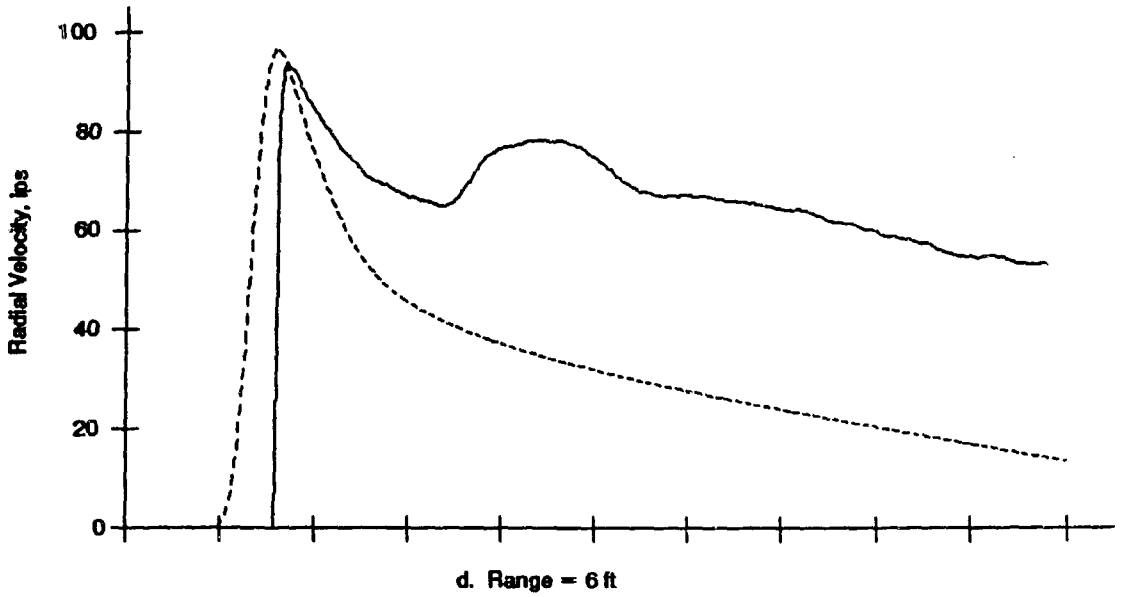

d. Range = 6 ft

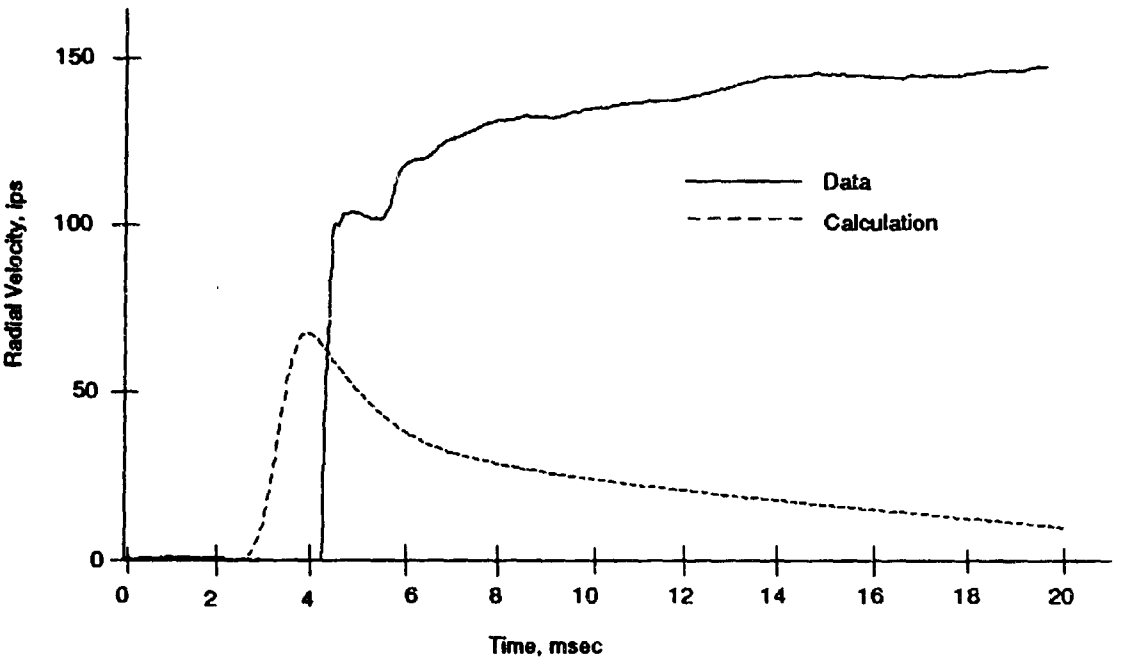

e. Range = 7 ft

Figure 33. (Concluded)

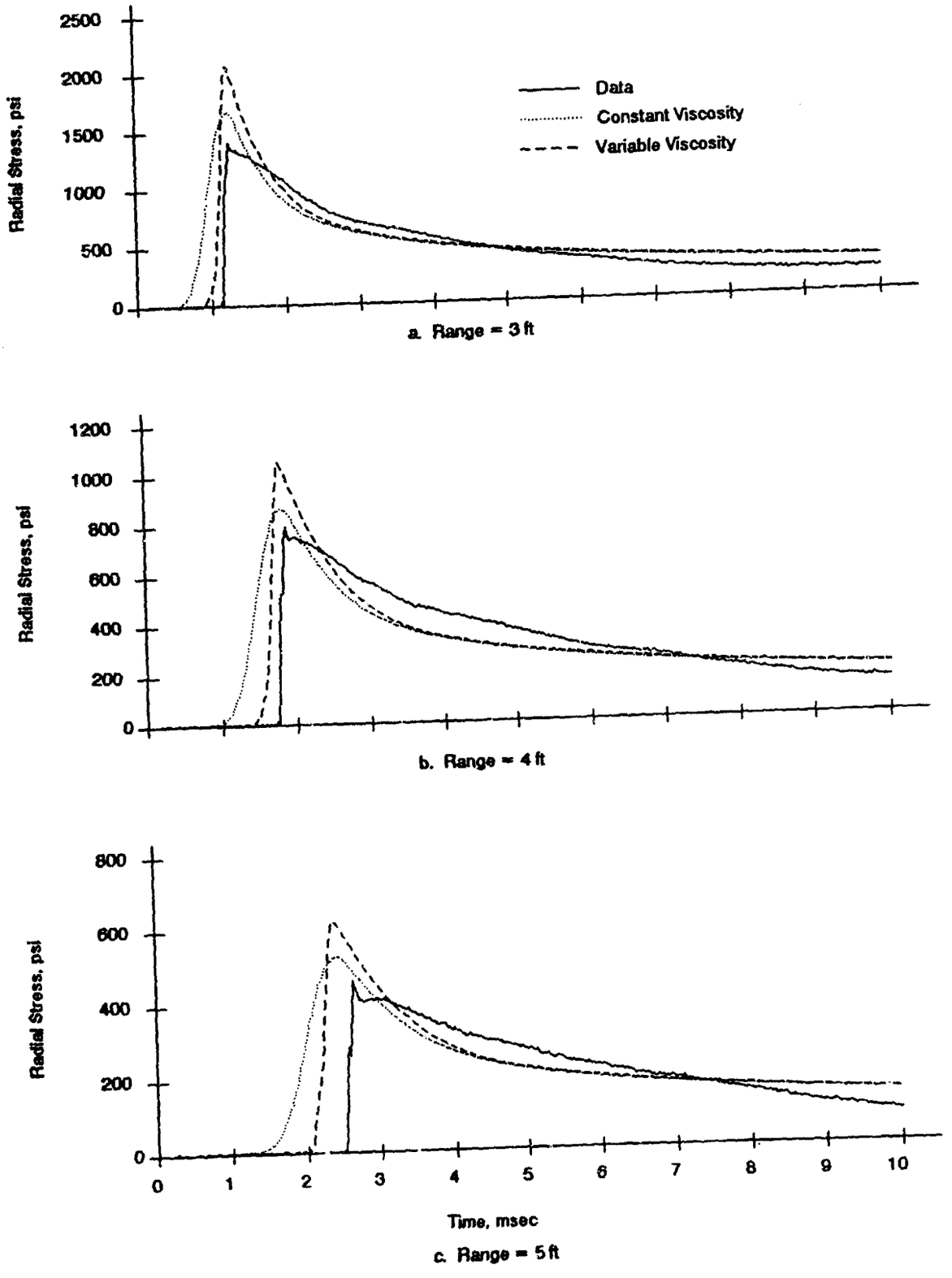

Figure 34. Effect of variable viscosity on stresses in sand (continued)

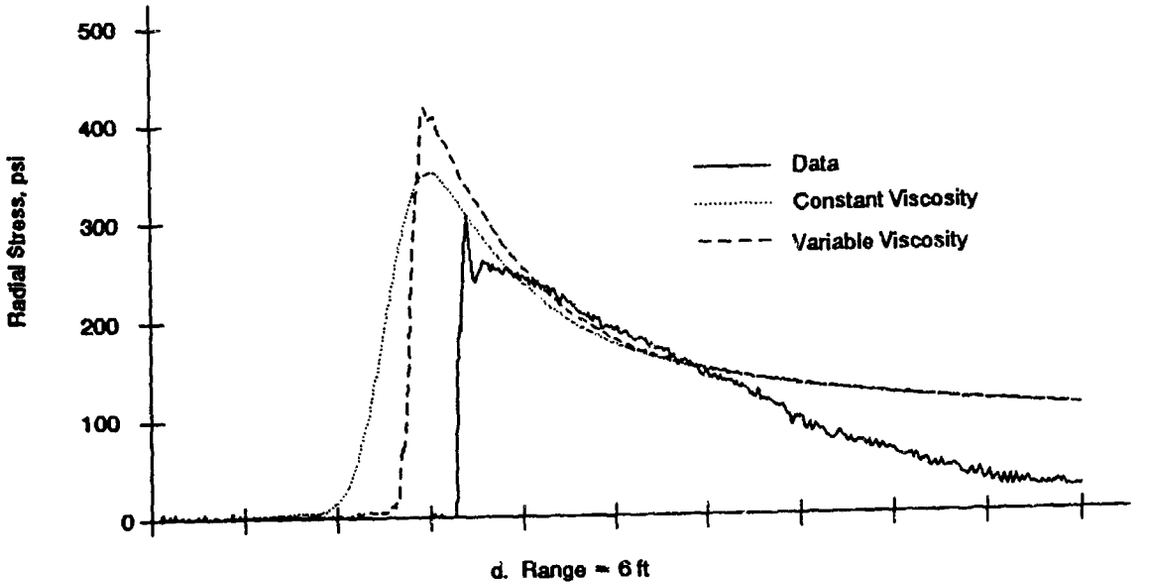

d. Range = 6 ft

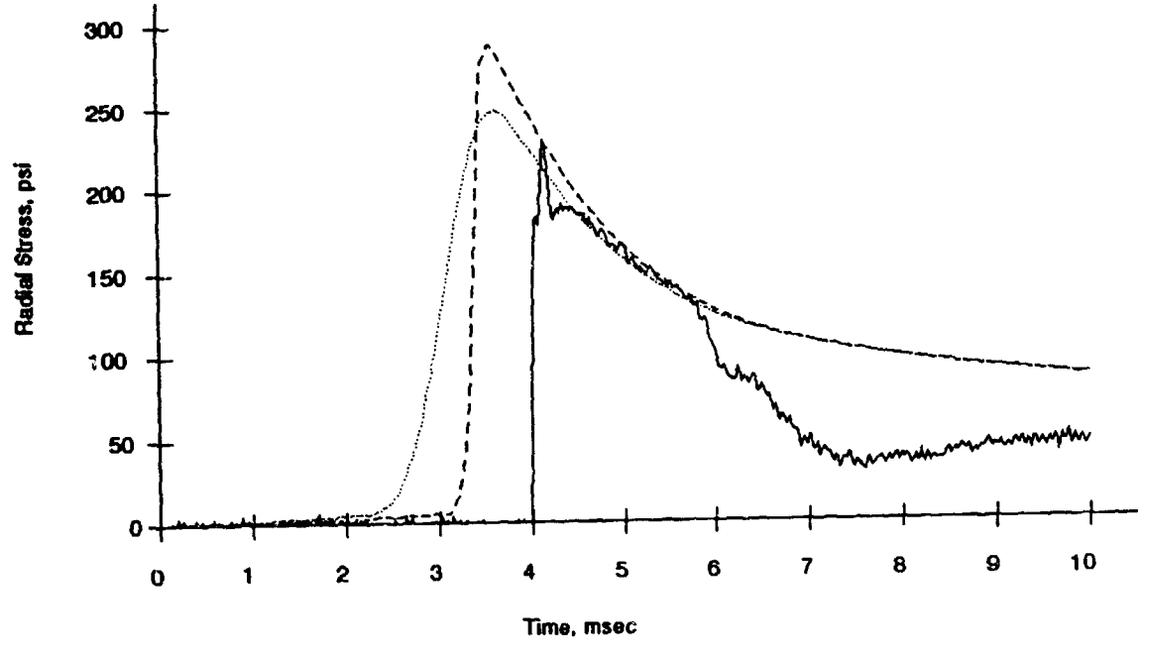

e. Range = 7 ft

Figure 34. (Concluded)

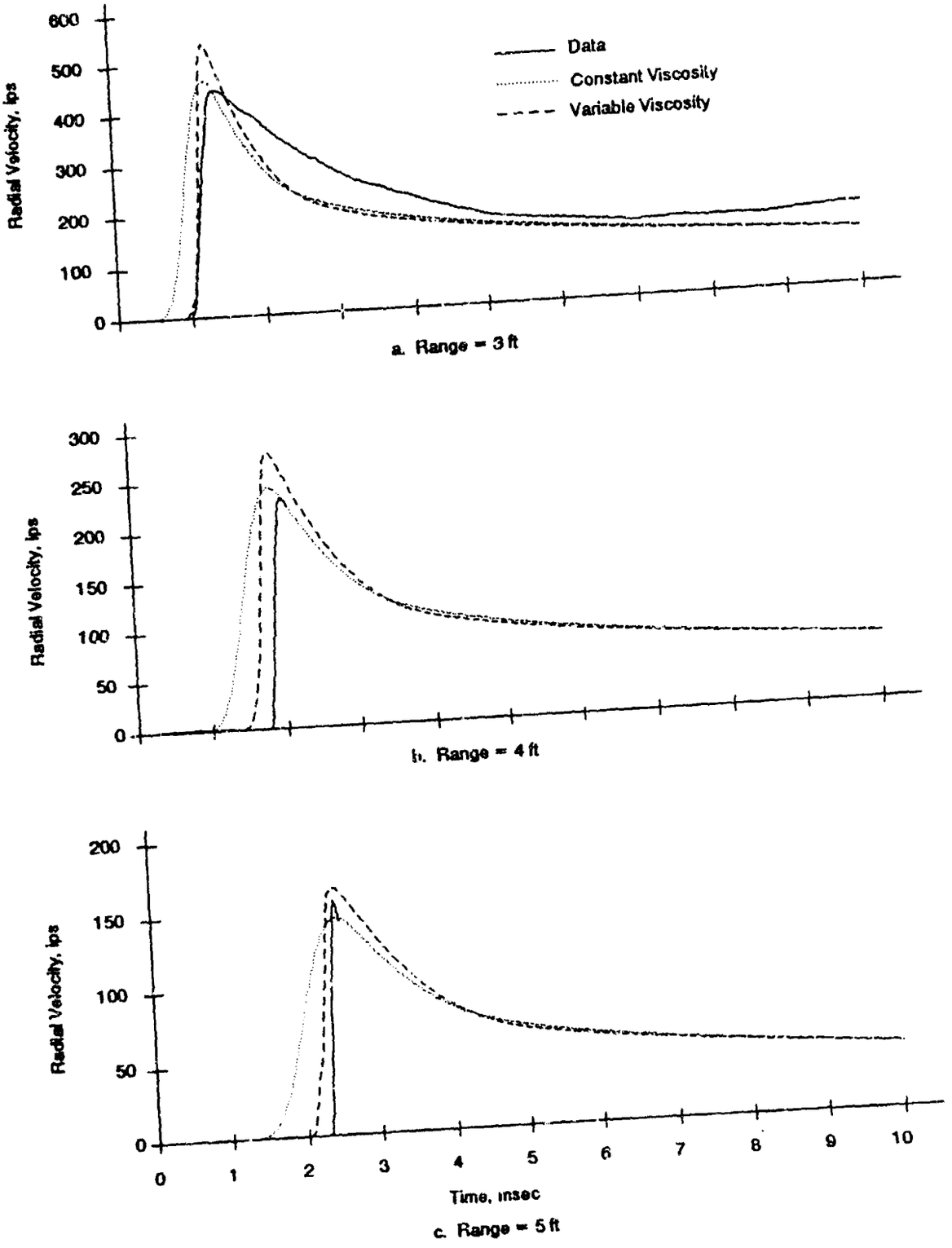

Figure 35. Effect of variable viscosity on velocities in sand (continued)

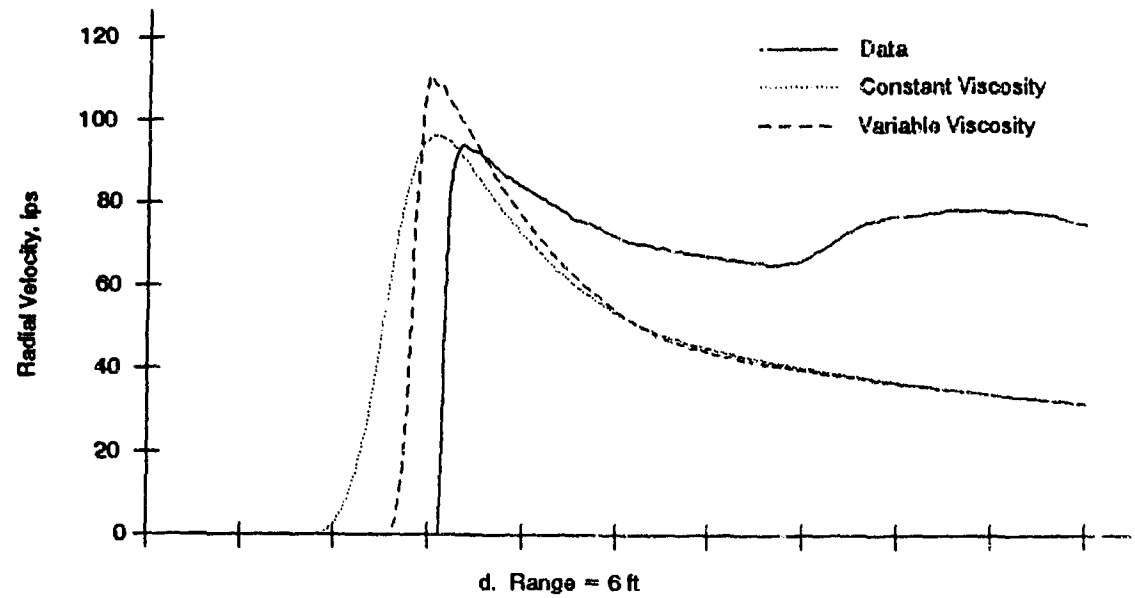

d. Range = 6 ft

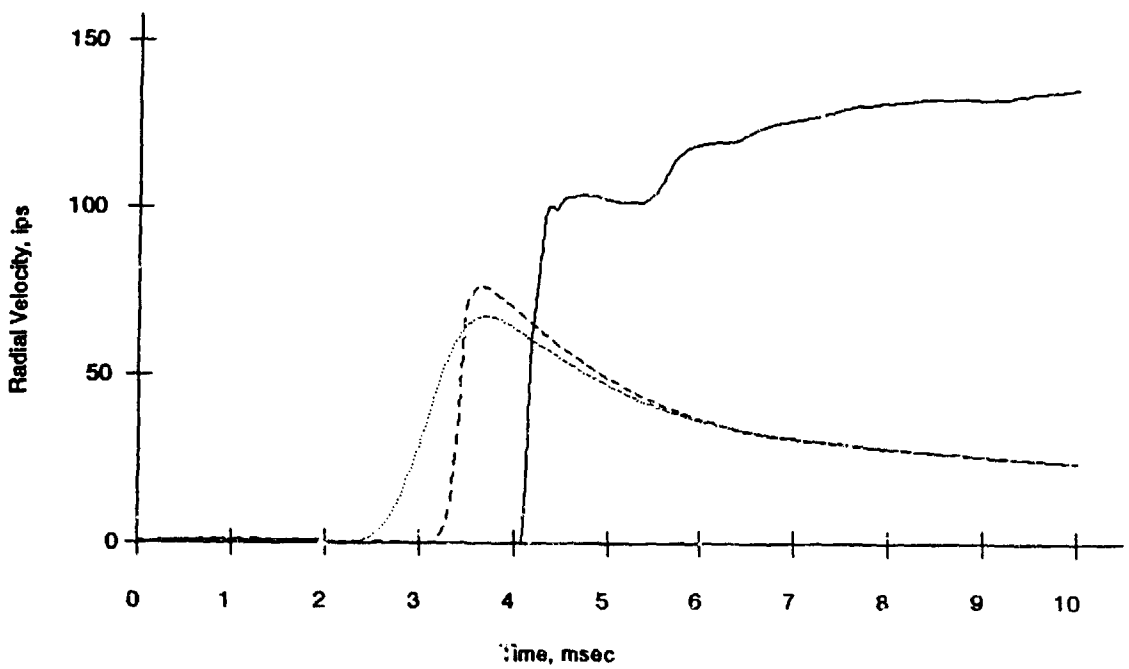

e. Range = 7 ft

Figure 35. (Concluded)

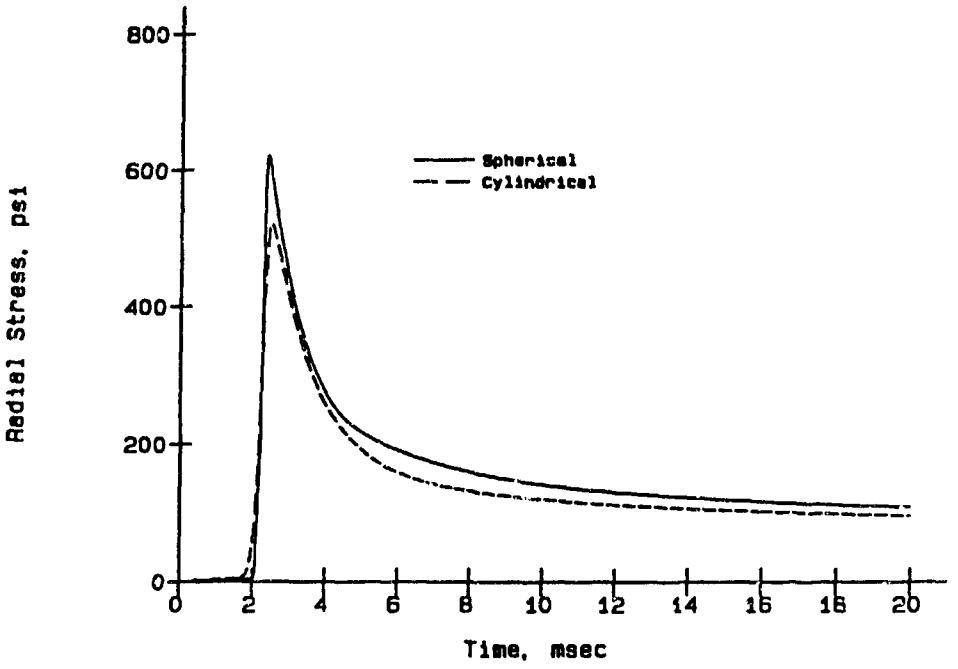

Figure 36. Comparison of cylindrical to spherical in sand, stresses at 5 ft

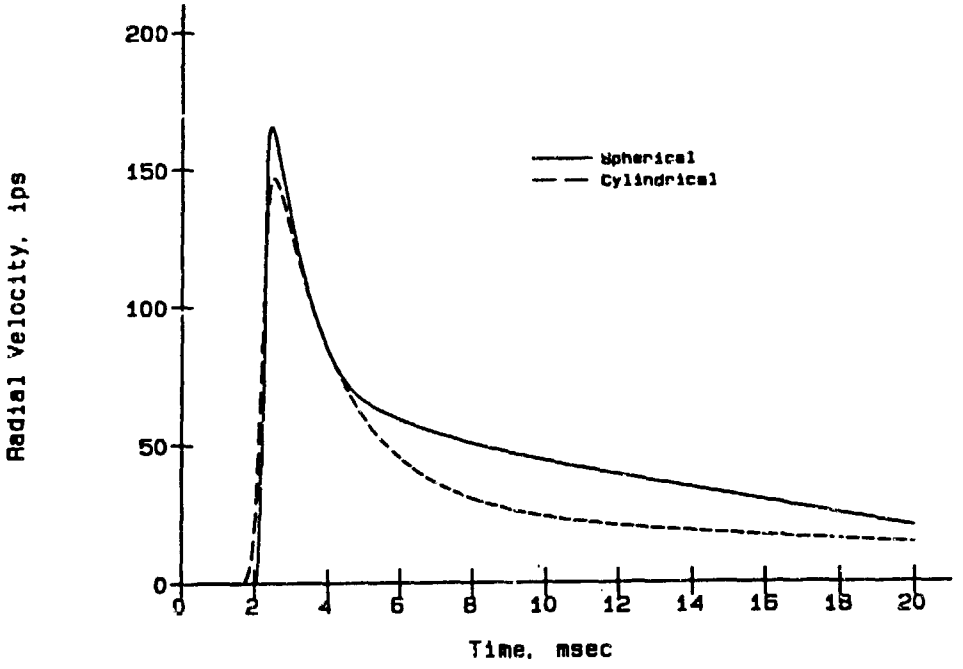

Figure 37. Comparison of cylindrical to spherical in sand, velocities at 5 ft

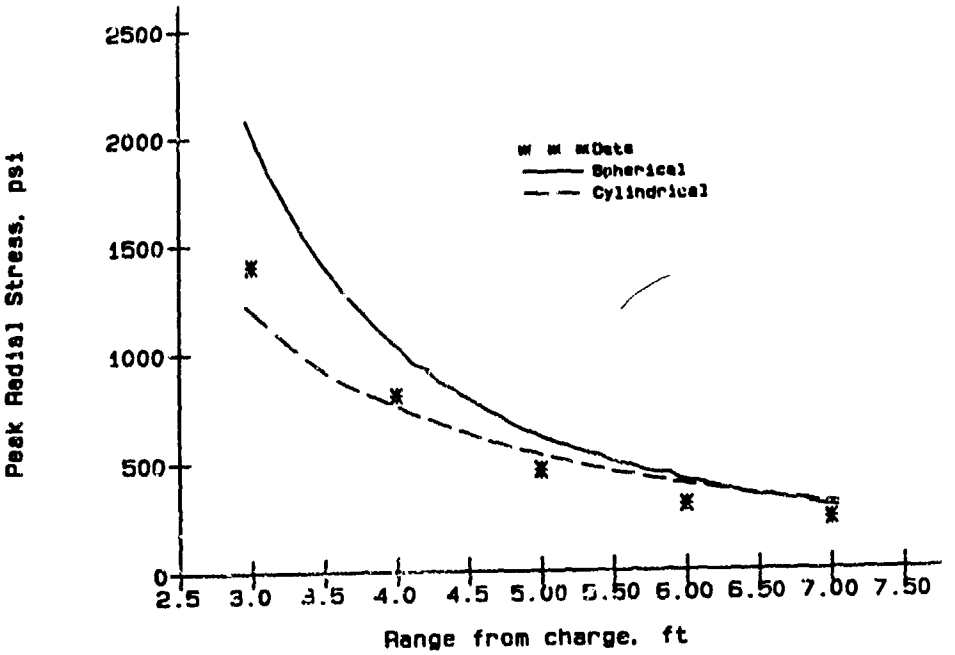

Figure 38. Comparison of cylindrical to spherical in sand peak stress versus range

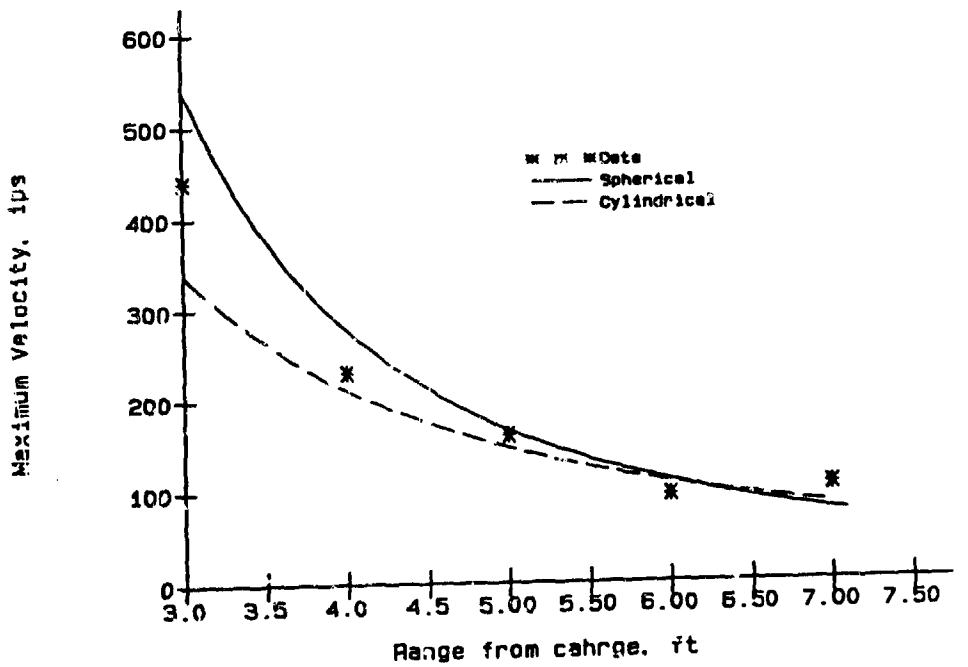

Figure 39. Comparison of cylindrical to spherical in sand, maximum velocity versus range

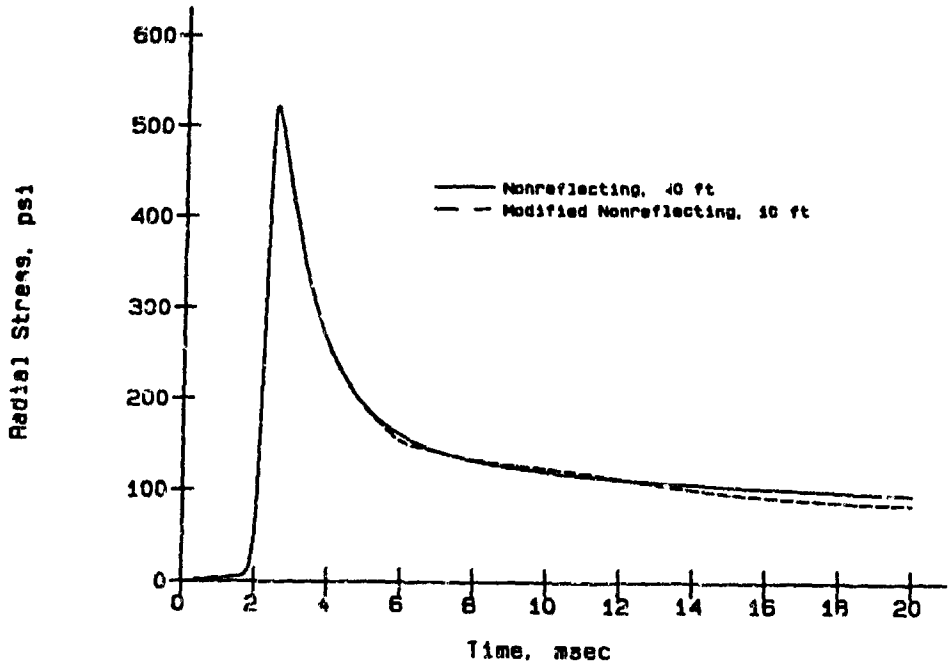

Figure 40. Effect of modified nonreflecting boundary on stresses at 5 ft in sand

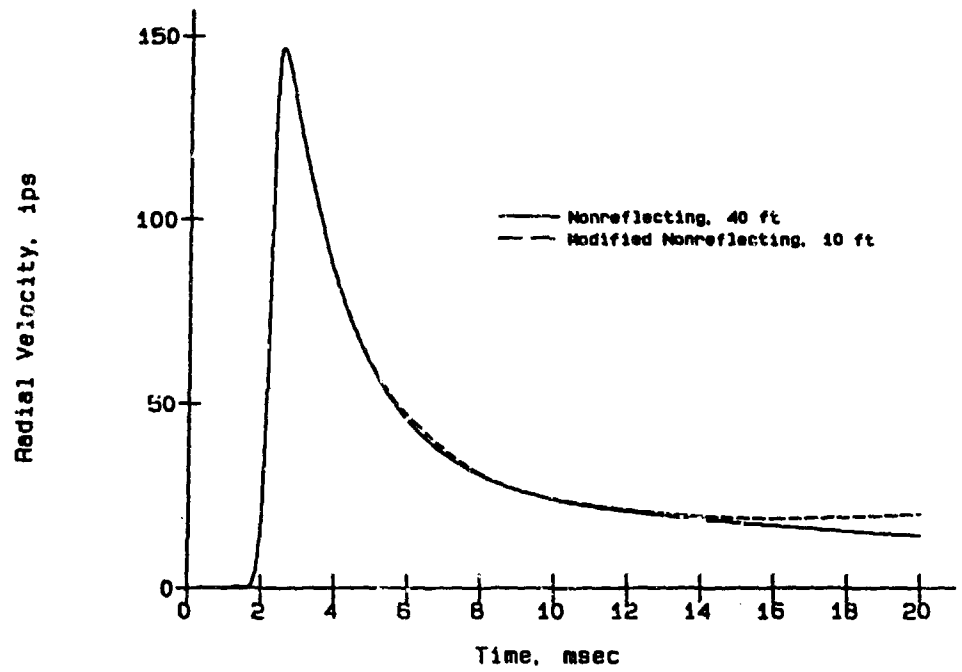

Figure 41. Effect of modified nonreflecting boundary on velocity at 5 ft in sand

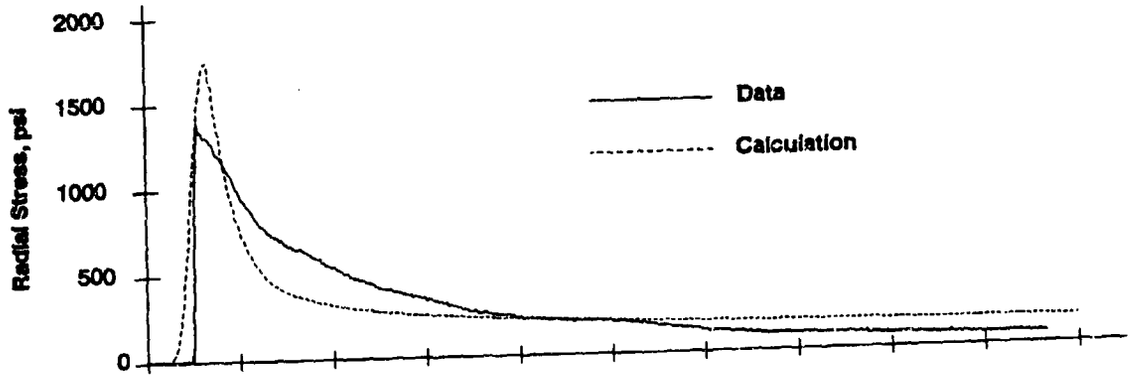

a. Range = 3 ft

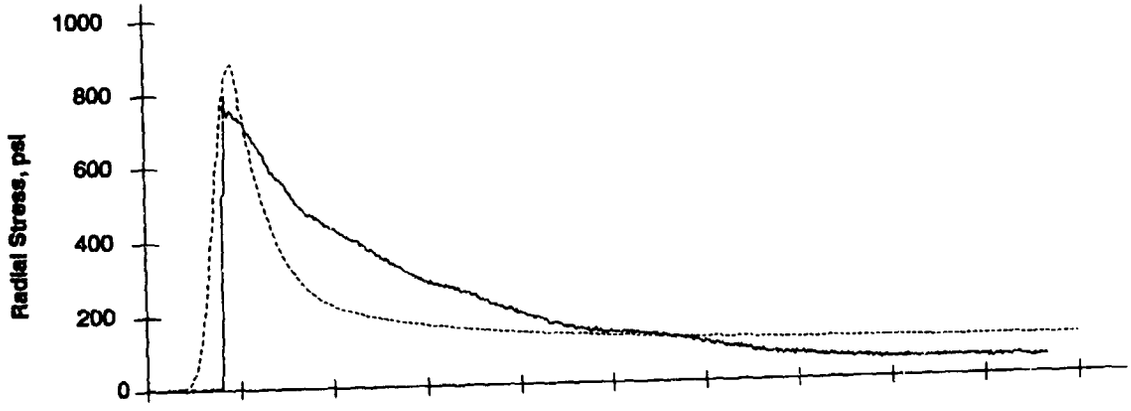

b. Range = 4 ft

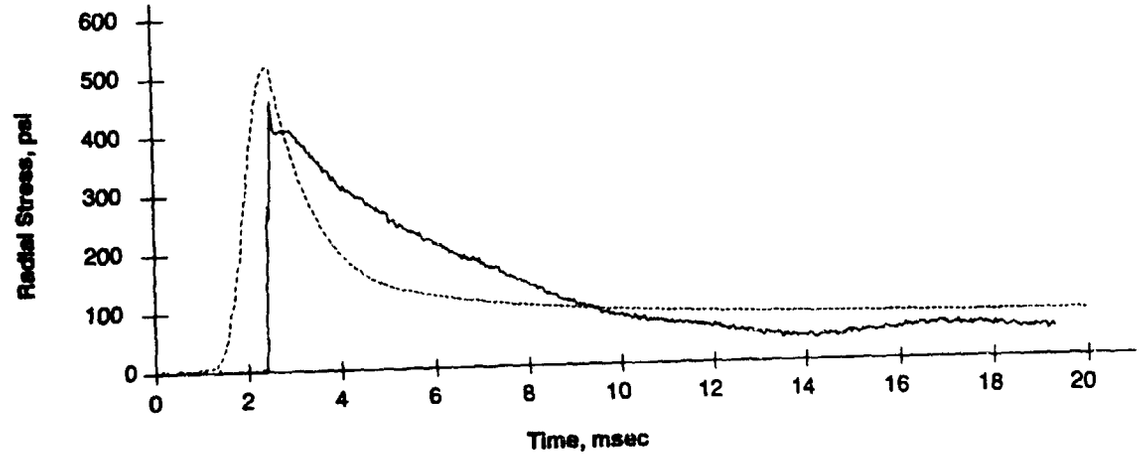

c. Range = 5 ft

Figure 42. Stresses computed using 8-node element for charge (continued)

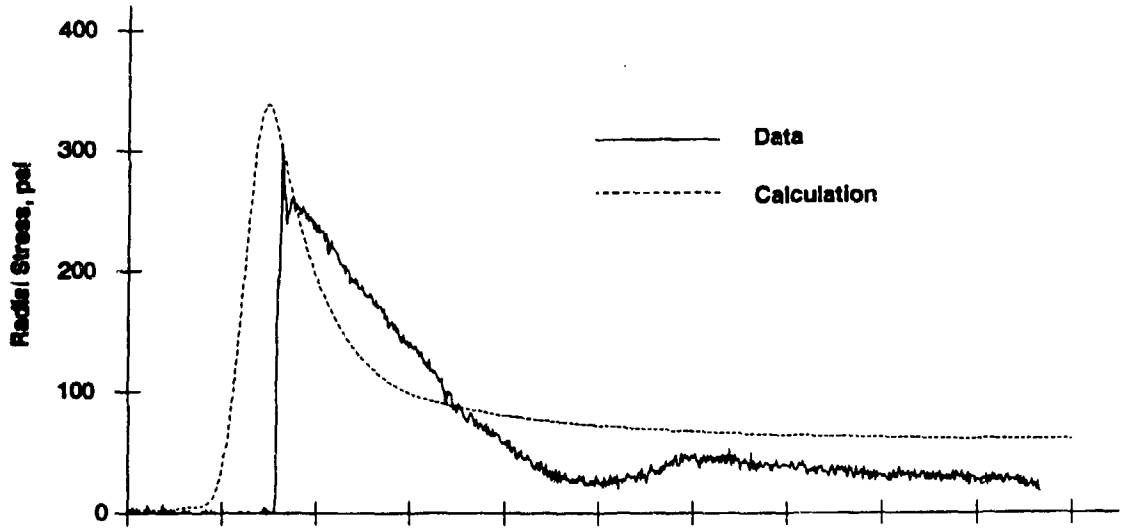

d. Range = 6 ft

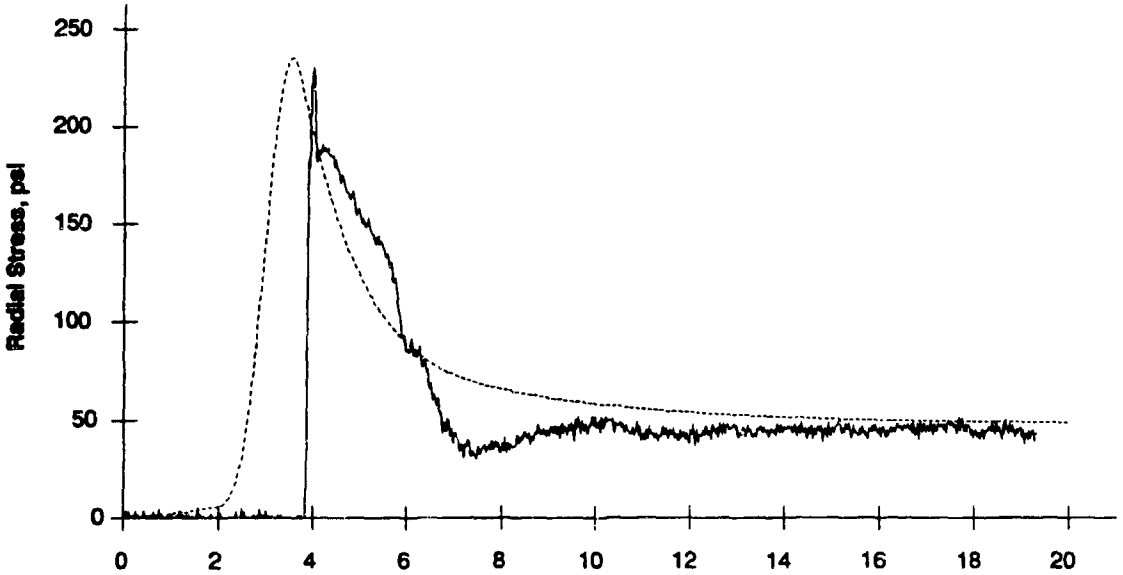

e. Range = 7 ft

Figure 42. (Concluded)

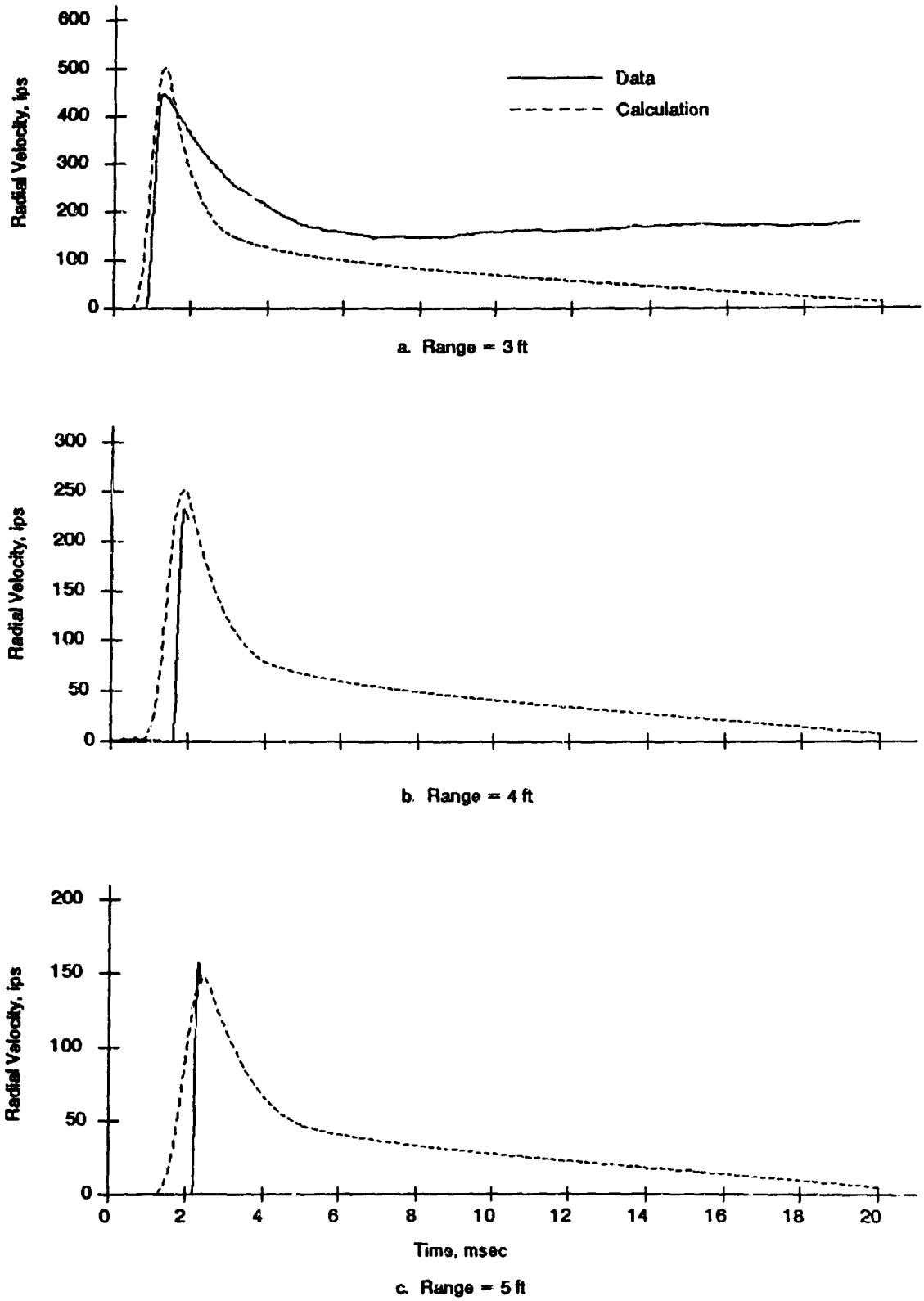

Figure 43. Velocities computed using 8-node element for charge (continued)

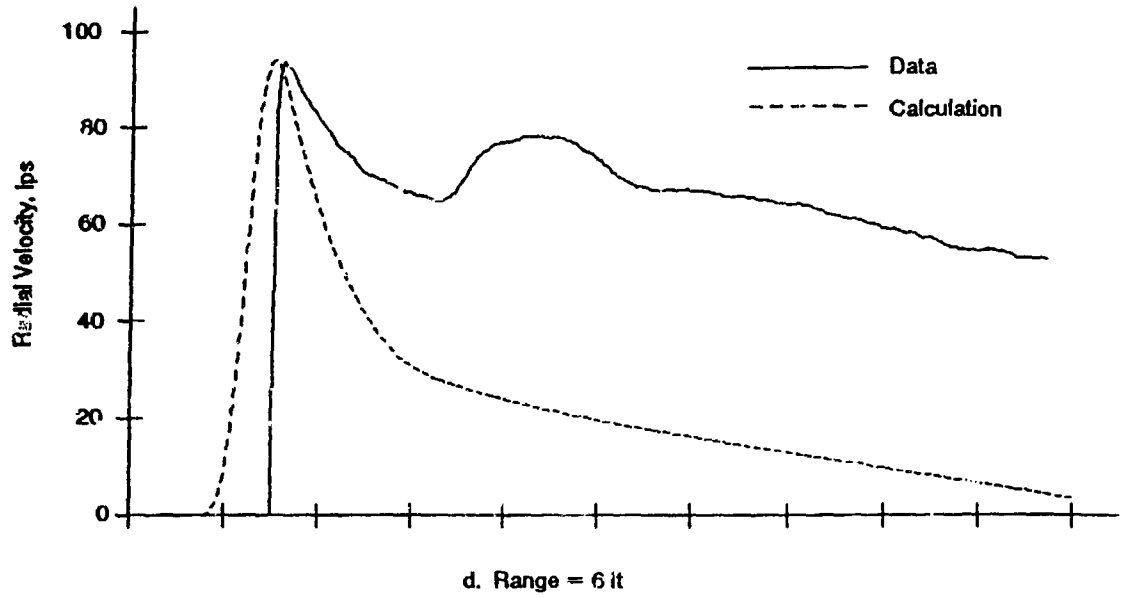

d. Range = 6 ft

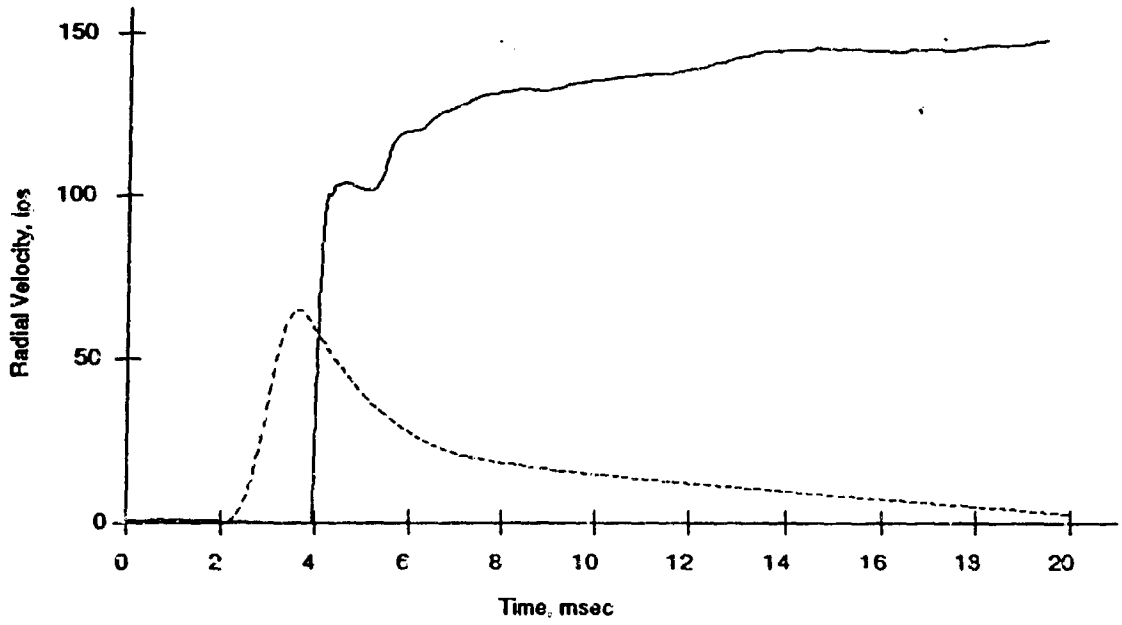

e. Range = 7 ft

Figure 43. (Concluded)

APPENDIX A: CALCULATION OF VOLUME OF SOLID ELEMENTS IN DYNA3D

1. In DYNA3D, the time-step for a given element is determined based on the dimensions of that element and the properties of the material of which that element is composed. The critical time-step is the smallest time-step of all of the elements making up the grid. If the charge is broken up into a large number of elements, the elements and, thus, the critical time-step would be very small. This small time-step would control the time-step for the FE analysis. If larger elements could be used for the charge, the critical time-step would increase and the analyses could be performed more efficiently.

2. The explosive is modeled using the JWL equation of state, which is accurate as long as the initial and current volume of the element are computed correctly. Since the volume can very easily be computed exactly, even for a severely distorted element, it was decided that the explosive could be modeled using only one element in the radial direction. For the 1-D spherical analyses, the charge was modeled using two tetrahedral elements.

3. The solid elements used in DYNA3D are constant strain trilinear hexahedral elements, as discussed in Hughes (1987). The DYNA3D user's manual (Hallquist and Benson 1987) states that 4-, 6-, and 8-node elements, such as those shown in Figure A1 may be used. This is an isoparametric element where the parent element (Figure A1) is mapped into the actual element geometry, which may have between four and eight nodes. The parent element is a cube with its center at the origin of the coordinate system, A. The coordinate of each of the corners is either plus or minus 1. For example, node 1 is at (-1, -1, -1), and node 7 is at (1, 1, 1).

4. The parent element is mapped into the solid element using the following relationships:

$$x(a, b, c) = \sum_{i=1}^{8} H_i x_i$$

$$y(a, b, c) = \sum_{i=1}^{8} H_i y_i$$

$$z(a, b, c) = \sum_{i=1}^{8} H_i z_i$$

where x_i, y_i, z_i are the x, y, and z coordinates of the ith node, and H_i is

the ith shape function given by:

$$H_i(a, b, c) = 1/8(1 + a_i a)(1 + b_i b)(1 + c_i c)$$

5. These same functions are also used to compute displacements in the parent element from the displacements of the node points, for example:

$$u(a, b, c) = \sum_{i=1}^{8} H_i u_i$$

where u is the displacement in the x direction

u_i is the x displacement of the ith node

The Jacobian of the transformation from the A system to the X system is given by:

$$J = \begin{bmatrix} x_{,a} & x_{,b} & x_{,c} \\ y_{,a} & y_{,b} & y_{,c} \\ z_{,a} & z_{,b} & z_{,c} \end{bmatrix}$$

where the comma indicates a partial derivative of the variable with respect to the subscript variable. For example:

$x_{,a}$ is the partial derivative of x with respect to a.

This Jacobian matrix, or its inverse, is used to compute nodal loads and strains in the element. Since this is a constant strain element, the strains may be computed at the origin of the parent element.

6. The original volume of the element is computed as the integral over the volume of the parent element of the determinant of the Jacobian matrix. The current volume may be computed using the current coordinates of the nodes in computing the Jacobian matrix. Consistent with using the strains at the origin of the parent system, the volume can be approximated using a single Gauss point at the origin. Thus, the volume is approximated as 8 times the value of the determinant of the Jacobian matrix, evaluated at the origin. The volume is computed exactly if the determinant of the Jacobian is constant or an odd function of the parent coordinates. If the determinant is neither a constant nor an odd function of the parent coordinates, the volume is only approximated.

7. For the elements used to model a 6-degree sector of a sphere with a radius of 4.0 in., the volume computed from the values of the determinants at the origins of the two elements is 0.08720 in. The actual total volume of the

two elements is 0.23180. Thus, the computed volume of the explosives is approximately 60 percent low.

8. Because the nodal loads are computed using similar procedures as used to compute the volume, the nodal loads are also computed incorrectly. This causes the deformations of the grid to deviate from spherical symmetry. The boundary conditions ensure that the nodes move along radial lines through the center of the charge but do not ensure that each node at a given radius moves the same amount. Apparently the nodes shared by the elements receive more load than the other two, since those shared nodes move faster. This difference in velocity is noticeable only in the nodes near to the charge, and there is very little difference at distances of interest in this study.

9. Given the method of computing volumes that is used in DYNA3D, it is important to be careful in developing the grid to be used for the explosives in these calculations. The error in volume can be reduced in several ways. In the calculations summarized in Part 3, a charge with a 6-in. radius was used. The additional volume caused by the increase in radius offsets the fact that the volume is undercomputed in the code. In this study the objective was to demonstrate that this method could be used to compute stresses and velocities at various ranges. Using the 6-in. charge is an acceptable way to demonstrate this.

10. Another way to minimize the volume error is to use a 5-node solid for the explosive. Even though the user's manual indicates that this element is not available, there is no reason why this element can't be used. Although no satisfactory calculations were performed using this element, the volume computed using DYNA3D is only 14 percent lower than the actual volume of the explosives, and displacements are spherically symmetric.

11. A third way to improve the volume calculation is to remove a small portion of the charge near the origin. Thus, the charge will be composed of a single 8-node element. If the inside 0.8 in. of the radius is removed, the volume computed by DYNA3D is 14 percent less than the desired volume of explosives. This is because there is very little volume inside of the portion removed, and the volume is computed much more accurately for the 8-node element. Analyses were performed using this method. The deformations were spherically symmetric, and the stresses and velocities agreed reasonably well with test data.

12. One problem with using this method is that it requires fixing all of the nodes on the inside radius of the charge. This causes no problems in these analyses. In the SST study, there will be a structure opposite the charge on one side, but there will be no structure on the other. This lack of symmetry could mean that the center of the charge could move. If all of the inside nodes are fixed, this is not possible.

13. Analyses were performed to look at the effects of using a cylindrically symmetric grid as compared to a spherically symmetric grid. In these calculations a 6-node solid was used. The volume of this element is computed correctly by DYNA3D, and cylindrically symmetric deformations occur. Thus, it appears that the 6-node element is performing satisfactorily.

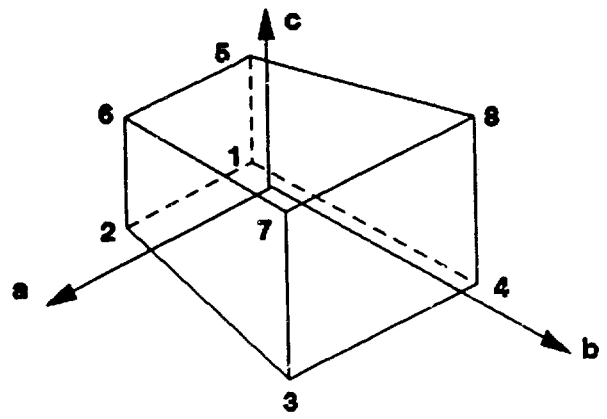

A = (a, b ,c)

Parent Element

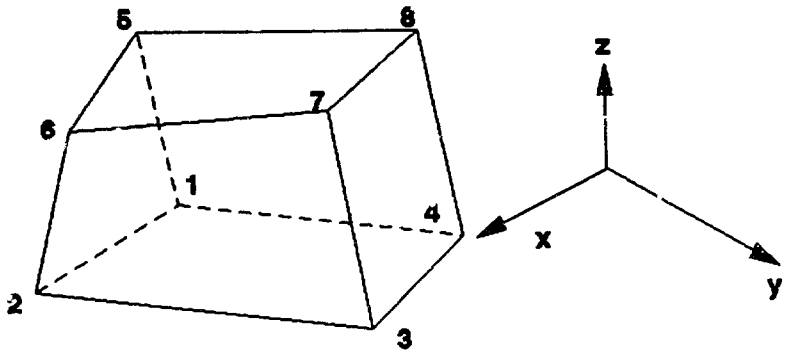

X = (x, y, z)

8 Node Solid

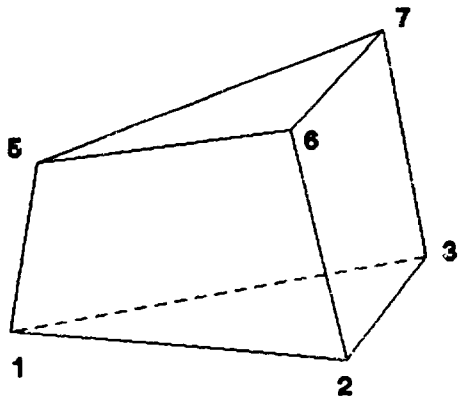

6 Node Solid

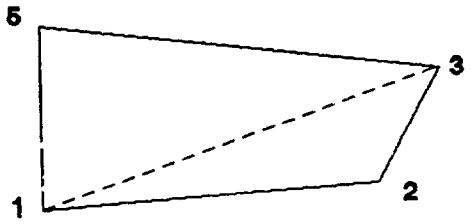

4 Node Solid

Figure A1. Solid elements available in DYNA3D